Tampere University

Kusti Saarinen

RADAR CHARACTERIZATION BASED ON FIELD TESTING

Master of Science Thesis
Faculty of Information Technology and Communication Sciences
Examiner: Taneli Riihonen
Examiner: Jaakko Marin
December 2025

ABSTRACT

Kusti Saarinen: Radar Characterization Based on Field Testing
Master's Thesis
Tampere University
Electrical Engineering
December 2025

This work concentrates on characterization process of a radar. Thesis has basic radar background for three different types of radars, including pulse radar, continuous-wave radar and multiple-input multiple-output radar. On top of that phenomena that affect all radars are also covered in this background. This background is required to understand how characterization process for radar can be done. Test cases demonstrated in this thesis are just few possible testing scenarios that can be utilized to characterize a radar. Characterization can be expanded significantly and different performance capabilities can be tested more thoroughly for more comprehensive results.

This characterization is partly done with anechoic chamber in a laboratory environment and partly done with field testing outside of controlled environment. This was done to extract performance data with controlled environment and in a real-world test scenario, where environment is not ideal and controlled. Test scenarios included in this thesis offered some understanding on the radar's performance. These tests provided data on how internal temperature affects the radar's performance, what the radar's transmit pattern looks like, what uncalibrated values mean in the radar's received signal data and how different resolutions affect the radar's performance. Temperature testing and transmit pattern testing was done in an anechoic chamber. Data calibration and resolution testing were handled with field testing.

Data gathered from these tests were analyzed to obtain real performance values for the radar. Temperature testing provided concrete results and transmit pattern was able to be measured accurately. Received data calibration was a success with accurate results. Last test case, resolution testing provided data that had a lot of fluctuation and therefore the results are not concrete, but they give a general idea on how changing resolutions affect the radar's performance. Other test cases provided data, which can be used to draw concrete results. This data was analyzed and maximum range was extrapolated for larger target.

Keywords: Radar, characterization, field testing

TIIVISTELMÄ

Kusti Saarinen: Tutkan karakterisointi kenttätestauksen avulla
Diplomityö
Tampereen yliopisto
Sähkötekniikka
Joulukuu 2025

Tässä työssä keskitytään tutkan karakterisointiin. Työn alussa esitellään kattavat perustiedot kolmesta eri tutkatyypistä, joihin sisältyy pulssitutka, jatkuva-aaltotutka ja moniantennitutka. Tämän lisäksi käsitellään ilmiöitä, jotka vaikuttavat kaikkien tutkien toimintaan. Tämä tausta pitää sisäistää, että karakterisointiprosessin voi ymmärtää. Työssä esitellään vain muutamia mahdollisia testiskenaarioita, joita tutkan karakterisointiin voidaan käyttää. Karakterisointia voitaisiin laajentaa merkittävästi ja eri suorituskykyparametrejä voitaisiin testata perusteellisemmin kattavampien tuloksien saamiseksi.

Karakterisointiprosessi suoritetaan osittain kontrolloidussa laboratorioympäristössä kaiuttoman huoneen avulla ja osittain kenttätestauksen avulla kontrolloimattomissa realistisissa käyttöympäristöissä. Molemmat tehtiin, koska haluttiin saada karakterisointia tehtyä sekä kontrolloidussa ympäristössä, että kontrolloimattomassa ympäristössä, jossa epäideallisuudet tulevat esiin. Työssä esitellyt testiskenaariot antoivat ymmärrystä tutkan suorituskyvystä. Näistä testeistä saatiin tietoa siitä, miten tutkan sisäinen lämpötila vaikuttaa sen lähetystehoon, miltä tutkan lähetyskuvio näyttää, mitä kalibroimattomat arvot vastaanotetussa signaalidatassa tarkoittavat ja miten eri resoluutioasetukset vaikuttavat tutkan suorituskykyyn. Näistä testeistä lämpötilatesti ja lähetyskuviomittaus tehtiin kaiuttomassa huoneessa. Vastaanotetun datan kalibrointi ja resoluutioiden vaikutus hoidettiin kenttätestauksella.

Testeistä kerättyä dataa analysoitiin ja siitä pystyttiin ratkaisemaan realistisia suorituskykyarvoja tutkalle. Lämpötilatestistä saatiin luotettavaa dataa ja lähetysantennikuvio saatiin mitattua tarkasti. Vastaanotetun datan kalibrointi onnistui hyvin tarkoilla tuloksilla. Viimeisen testin, eli resoluutiotestin tapauksessa data oli niin vaihtelevaa, että niistä ei suoraan voi antaa tarkkaa arviota suorituskyvystä, mutta se antoi hyvää yleisymmärrystä siitä, että miten resoluutioiden muuttaminen vaikuttaa kyseisen tutkan suorituskykyyn. Muiden testien datat olivat hyvin selkeitä ja niiden avulla pystyi johtamaan lopullisia tuloksia. Tätä dataa analysoitiin ja sen avulla ekstrapoloitiin maksimaalinen havaitsemisetäisyys isommalle kohteelle.

Avainsanat: Tutka, karakterisointi, kenttätestaus

USE OF AI IN THESIS

I have utilised AI tools in my thesis:

☐ No
☒ Yes

The AI tools utilised in my thesis and their purposes are described below:

Names and versions of AI tools: ChatGPT-5 and ChatGPT-5 Mini

Purpose of using AI tools: Help with finding references for thesis

Sections where AI tools were used: Radar theory

I acknowledge that I am fully responsible for the entire content of my thesis, including the parts generated by AI, and accept accountability for any violations of ethical standards in publications.

PREFACE

Radar characterization is very versatile field, which requires a lot of knowledge on radars and signal processing. This thesis with all testing included took approximately 6 months to finish.

I want to thank everyone who helped me with this thesis process, especially Jaakko Marin and Taneli Riihonen for guidance. I would also like to thank everyone else who helped me during this thesis process, mainly my co-workers, and of course my employer Saab Finland Oy for this amazing opportunity.

Tampere, 15 December 2025

Kusti Saarinen

CONTENTS

LIST OF SYMBOLS AND ABBREVIATIONS

A	carrier amplitude
a	amplitude
a_p	attenuation on path p
a_{th}	CFAR threshold scaling factor
B_{chirp}	chirp bandwidth
B_{N}	noise bandwidth
c	speed of light
d_{ant}	distance between two antenna elements
$\underline{E_J}$	scattered electric field strength returned to radar
$\underline{E_S}$	incident electric field strength at target
f	instantaneous frequency
f_{B}	beat frequency
f_{c}	carrier frequency
f_{d}	Doppler frequency shift
f_{m}	frequency modulation applied
F_{n}	noise factor
G_{AGC}	adaptive gain control gain
G_{i}	integration gain
G_{R}	receiver antenna gain
G_{T}	transmit antenna gain
H	CFAR local detection threshold
h	channel
i	FFT index
i_{max}	FFT index that results in maximum value
k	Boltzmann's constant
k_{f}	frequency modulation multiplier
k_{p}	phase modulation multiplier
λ	wavelength
l_{r}	location of receiving antenna
l_{t}	location of transmit antenna
l_{v}	location of virtual antenna
L_{a}	additional losses
L_{T}	thermal loss
$m(t)$	message signal
m	sample
M	number of signal samples
n	distance in number of elements
N_{ant}	number of antennas
N_{chirp}	number of transmitted chirps
N_{r}	number of receivers
N_{t}	number of transmitters
N_{T}	number of training cells used
P_{avg}	average power
P_{N}	noise power
P_{pk}	peak power
P_{R}	received power
P_{T}	transmit power
R	distance to a target
R_{cr}	range measured from a corner reflector

R_{det}	range value from a detection
R_{M}	range multiplier
R_{min}	minimum range
R_{tr}	distance between transmitter and receiver
$\mathrm{RCS}_{\mathrm{cr}}$	RCS measured from a corner reflector
$\mathrm{RCS}_{\mathrm{est}}$	RCS estimate
SNR_{100}	SNR value estimated for a larger target
$\mathrm{SNR}_{\mathrm{cr}}$	SNR value measured from a corner reflector
$\mathrm{SNR}_{\mathrm{det}}$	SNR value from a detection
$\mathrm{SNR}_{\mathrm{th}}$	SNR threshold
T	temperature
T_{r}	temperature sensor reading
t	time
t_{chirp}	chirp length in time
t_{i}	integration period
t_{m}	modulation time
t_{tr}	switching time
τ	propagation delay
τ_p	propagation delay on path p
τ_{t}	transmit period
v_{r}	target's radial speed
x	transmitted baseband signal
x_p	transmitted signal on path p
x_m	signal power in cell m
x^*	transmitted baseband signal's complex conjugate
$\bar{x}$	transmitted signal
$\bar{x}^*$	transmitted signal's complex conjugate
y	received signal
$\bar{y}$	received baseband signal
y_{cc}	cross-correlation of received and transmitted signal
$\mathrm{z_i}$	interference
$\mathrm{z_w}$	thermal noise
θ	angle of arrival
θ_{E}	elevation angle of arrival
θ_{EST}	angle of arrival estimation
θ_{FOV}	field of view
θ_n	angle of arrival from two antenna elements n-elements apart
θ_{RES}	angle of arrival resolution
Φ_{B}	phase shift between transmitted and received signal
Φ_n	phase shift between two antenna elements n-elements apart
φ	frequency or phase modulation

ADC	Analog-to-digital converter
AGC	Adaptive Gain Control
AM	Amplitude Modulation
CA-CFAR	Cell Averaging Constant False Alarm Rate
CW	Continuous-Wave
FDM	Frequency-Division Multiplexing
FFT	Fast Fourier Transform
FM	Frequency Modulation
FMCW	Frequency Modulated Continuous-Wave
FOV	Field Of View
FSPL	Free-Space Path Loss
GOCA-CFAR	Greatest-of Cell Averaging Constant False Alarm Rate
LFM	Linear Frequency Modulation
LNA	Low Noise Amplifier
LO	Local Oscillator
MIMO	Multiple-Input and Multiple-Output
MISO	Multiple-Input and Single-Output
PA	Power Amplifier
PM	Phase Modulation
PRF	Pulse Repetition Frequency
PRI	Pulse Repetition Interval
RCS	Radar Cross Section
RX	Receiver
SCR	Signal-to-Clutter Ratio
SDR	Software-Defined Radio
SIR	Signal-to-Interference Ratio
SNR	Signal-to-Noise Ratio
SOCA-CFAR	Smallest-Of Cell Averaging Constant False Alarm Rate
TDM	Time-Division Multiplexing
T/R	Transmitter/Receiver
TX	Transmitter

1. INTRODUCTION

Radar is a device that is designed for detecting and ranging objects with electromagnetic waves. That can also be seen in the name, because the word radar is short for radio detecting and ranging. Radars have been in use for a long time, radar history ranges all the way back to 1865 when James Clerk Maxwell developed his electro-magnetic-light theory. Ever since then different types of radars have been implemented and nowadays radars are used in many diverse fields and tasks, including but not limited to: air traffic control and aircraft navigation, ship navigation and safety, law enforcement and agriculture. All of these use some radar system to help in the task. Every field and application requires special characteristics from the radar that is used, therefore different types of radars have been developed and nowadays there is a very wide range of different types of radars which all have different use-cases and purposes. In this thesis we will be taking a more in-depth look at a limited number of these radar types, based on their relevance in today's radar technology. [1][2]

Radar characterization is important, because it gives performance values for the radar. These values will help to understand performance and see if the radar is suitable for designed use case. There are many companies like Novelic and Intersoft Electronics, which offer radar characterization services. These services are able to evaluate or validate radar characteristics with field testing or target simulation services. These tests are usually done with high-end purpose-built devices that are used to mimic different targets and scenarios. Field testing is testing, which is done outside of controlled laboratory environment and therefore has more non-idealities. In this thesis, aim is to do radar characterization testing on the field and provide data on radar characteristics in house. Field testing is a vital part of radar testing, because it can be used to determine if radar suits the designed use case. Field testing is used for radar characterization in this thesis, because large enough antenna measurement chamber was not available and radar real life performance has to be evaluated. Field testing provides a great solution to evaluate how the radar works in use cases that the radar is designed for. [3]

In this thesis we design a field testing setup that is suitable for radar characterization and use it to obtain empirical data on the radar sensor considered for this thesis. Then we will analyze test results and compare them with theoretical specifications for the radar. Radar characterization will be documented in this thesis in a way that brings up different

testing methods that were done to extract real-world performance data from a radar that was investigated for this thesis. Tests done in this thesis include testing how internal temperature affects the radar's transmit power, measurement of transmit antenna pattern, calibration of radar's received signal data with corner reflector measurement and testing how different resolutions affect the radar's performance.

Results from field testing proved to be very useful in analyzing the radar's performance and provided useful data which can be used to evaluate how well radar would work for real life scenarios. One example for this is the temperature behaviour, from those results we were able to see that transmit signal power lowers 3 dB when internal temperature reaches $65\ ℃$.

The remainder of the thesis is organized as follows. Chapter 2 will include radar background to show mathematical models behind radar phenomena and processing on general level. This theory will be described more deeply for 3 types of radars, after that, common algorithms used with radars will be introduced. Chapter 3 will introduce the radar used for thesis and first characterization tests. Chapter 4 will display field testing scenario and results from the measurement campaign.

2. RADAR THEORY

This chapter presents radar theory that explains how radars work. Radars have different types of limitations and phenomena that affect their performance. Radars typically operate either by transmitting continuously or with pulsed signals, and therefore there are many aspects that can have an effect on radar performance based on its type. Information here will be required to understand the advantages and disadvantages for different radar types. In this part we will cover basic radar equations, that apply for all radars. We will also go more in-depth with few types of radars; pulse radar, continuous-wave (CW) radar, frequency-modulated continuous-wave (FMCW) radar and multiple-input and multiple-output (MIMO) radar.

Radars work by sending an electromagnetic energy signal in the air. This signal then reflects off of an object and a small portion of that energy is returned back to the radar, where it is received. Then depending on type of radar system, different calculations happen. Pulse radars for example calculate how much time it took for the signal to return from an object back to radar. This basic principle works the same as sound reflection, where if you shout at woods or other sound reflecting objects, it will echo back to you. Calculating the time it took for the echo to reach you, you can calculate the distance. For radars, depending on the type of radar used, it can also find out directions, velocities and other data from detected objects. All of this is based on the returning echo and calculations that can be done from that returning energy. [1][2]

Radars usually have transmitter and receiver spaced closely together, however it is also possible to have them separated by a long distance. Radars with transmitter and receiver closely together are called monostatic radars and equations below apply to them. Bistatic radars have transmitter and receiver separated with a significant distance and they have different channel characteristics, because instead of relying on distance between radar and an object, we need a distance between a transmitter and an object and then distance from the object to a receiver. Bistatic setup changes channel calculations, but radar investigated in this thesis is a monostatic radar. The radar used here is a FMCW MIMO radar operating on 17 GHz frequency. The radar utilizes linear frequency modulation (LFM). Signal parameters used in the radar are not fixed and can be changed. [4]

2.1 Basic Radar Principles

Radars operate by transmitting an electromagnetic signal in the air and then receiving an echo of that signal. For this to happen we need to have a transmitter (TX) and a receiver (RX) in a radar system. Depending on the type of the radar, these can have very different specifications and functionalities, but one thing they all have in common is that they are there to transmit and receive the signal used for sensing objects.

2.1.1 Radar Signal

While radars can differ radically both in architecture and transmitted waveforms, there are equations that apply to them all, because they all rely on electromagnetic signals that travel over the air. Radar transmit waveforms can be generally modelled as:

$$\bar{x}(\mathrm{t}) = a(t)\cos\left(2\pi f_{\mathrm{c}} t + \varphi(t)\right) \tag{1}$$

where $a(t)$ represents amplitude of the carrier signal, term f_{c} is carrier frequency in Hertz and term $\varphi(t)$ is used to model frequency or phase modulation in carrier signal. Carrier signal itself is a high-frequency sinusoidal signal, that is used to carry our modulated baseband signal. Overbar on x tells that this signal is on carrier frequency and not de-modulated. [4]

Transmitted signal will travel over the air, which acts as a channel for our signal. This channel affects the signal and changes its properties. To estimate these changes, we need a channel model. Equations below apply only for monostatic radars. Channel model used depends on type of radar and environment. Our received signal from this channel can be written as:

$$\bar{y}(t) = \left(\sum\nolimits_p a_p(f,t)\bar{x}\left(t-\tau_p\right)e^{\mathrm{j}2\pi f_{\mathrm{d},p} t}\right) + \mathrm{z_w}(t) + \mathrm{z_i}(t) \tag{2}$$

where $\bar{y}(t)$ is our received signal combined from all paths. $a_p(f,t)$ is our attenuation and $\tau_p(f,t)$ is our propagation delay on frequency f at time t on path p. Frequency shift caused by Doppler effect on the path p is $f_{\mathrm{d},p}$. Doppler shift will be introduced more in depth in this thesis. The transmitted signal is $\bar{x}$ and signal's instantaneous frequency during time instant t is f. On top of this there is also thermal noise $\mathrm{z_w}$ and interference $\mathrm{z_i}$. Attenuation includes all factors, like antenna attenuations and attenuation because of distance. [5]

All electromagnetic signals attenuate over a distance, most common model for this attenuation is free-space path loss (FSPL), which is how much signal strength decreases over a range in a vacuum for isotropic radiator. Equation for this is:

$$\mathrm{FSPL} = \left(\frac{4\pi R_{\mathrm{tr}} f}{\mathrm{c}}\right)^2 \tag{3}$$

where R_{tr} is distance between transmitter and receiver, f is frequency used and c is speed of light. However, in case of radar we are usually interested in full path loss, because our signal has to reflect back to a receiver from an object. Because of this our FSPL equation changes to:

$$\mathrm{FSPL} = \left(\frac{4\pi R f}{\mathrm{c}}\right)^4 \tag{4}$$

where R is distance to an object. FSPL for a radar increases significantly over range, because signal has to travel twice as far. This causes exponent to grow from 2 to 4. [6]

We can estimate these effects in terms of signal strength with the well-known radar range equation. This equation is widely used to estimate strength of the received signal:

$$P_{\mathrm{R}} = \frac{P_{\mathrm{T}} G_{\mathrm{T}} G_{\mathrm{R}} \lambda^2 \mathrm{RCS}}{4\pi^3 R^4 L_{\mathrm{a}}} \tag{5}$$

Variables used in radar range equation are as follows: received signal power P_{R}, transmitted signal power P_{T}, transmitter antenna gain G_{T}, receiver antenna gain G_{R}, signal's wavelength λ, target's Radar-Cross-Section (RCS) and additional losses from radar hardware and other sources L_{a}. All variables in this equation are in linear units. This equation is used to calculate how much power the received signal has at the receiver antenna output. This radar range equation uses FSPL calculated in equation (4) as a part of it. [4]

All of the parameters in the radar range equation have an effect on our detecting capability. Some variables can be tuned to make our radar perform better, but most variables are tied to our mission, like RCS and range. Range especially is a very significant variable, as strength of a received signal decreases rapidly as our range increases. This is why high-transmit-power radars are needed to detect objects that are far away.

RCS itself is not a simple parameter, RCS describes the ability of an object to radiate energy back to radar. This can be said as being the detectability of an object with a radar. Bigger the RCS, the easier an object is to detect with a radar. RCS is defined as:

$$\mathrm{RCS} = 4\pi R^2 \frac{\left\|\underline{E}_{\mathrm{S}}\right\|^2}{\left\|\underline{E}_{\mathrm{I}}\right\|^2} \tag{6}$$

Where $\underline{E}_{\mathrm{S}}$ is the incident electric field strength at the target and $\underline{E}_{\mathrm{I}}$ is the scattered electric field strength returned to radar. Unit used for RCS is m^2, where $1\ \mathrm{m}^2$ means equal RCS to an ideally reflecting sphere that has same radius as a circle with an area of $1\ \mathrm{m}^2$. [5]

RCS is related to electric field strengths, which means that RCS is not only defined by an object's size, but also includes material that object is made of and angle (unless object is a sphere). Objects that have a complex shape can have a very different RCS depending on the orientation, especially when different materials are used throughout the object. Even a small change in target's orientation has a huge impact on RCS. This causes RCS to fluctuate for most targets. Different materials can also make very big changes in RCS depending on the TX-signal frequency, so when RCS is being calculated or tested for an object, it needs to be done with the radar's operating frequency. [5]

Simulating RCS is very complex task and because of that, usually estimates are used for objects RCS. Some simple shapes are easier to calculate and simulate RCS for, such as sphere. Complex objects have many individual scatters echoing back to radar at different signal levels and this makes RCS simulation a hard task. For this purpose, corner reflector with known RCS value is typically used for radar characterization. [5]

2.1.2 Noise And Clutter

Noise is one of the key challenges to overcome with every radio system. Most relevant noise source is thermal noise, which can be calculated with equation:

$$P_{\mathrm{N}} = kTB_{\mathrm{N}} \tag{7}$$

In this equation P_{N} is noise power, k is Boltzmann's constant, T is noise temperature and B_{N} is noise bandwidth. Boltzmann's constant is a relation between object's energy and temperature, $k = 1.380649 * 10^{-23}\, J/K$. This equation gives us the noise floor, which is an average of the noise power over time. [7][8]

Other noise sources include cosmic radiation, atmospheric noise and noise from electronics. For radar investigated in this thesis, the most relevant additional noise source for us is electronic noise. Non-idealities in electronics add noise to our system and it can be represented with noise factor F_{n}. Noise factor means how much a device or a component adds to received noise. Amplifiers especially are a problem, because they amplify the whole signal, which includes the noise. Noise factor is defined as:

$$F_{\mathrm{n}} = \frac{\text{total noise at output}}{\text{total noise at input}} \tag{8}$$

In this case, noise factor is how much the radar is adding noise on top of the existing noise. [9]

Cosmic radiation is any radiation that comes from space, it can originate from the Sun, other stars or cosmic microwave background. These noise sources affect different fre-

quencies differently. Cosmic radiation is crucial when using systems that utilize a frequency under 2 GHz. Atmospheric noise origins from radiation during lightning discharges. Lightning discharges cause atmospheric noise that is relevant on frequencies that are under 30 MHz. Carrier frequency used (17 GHz) means that these are not relevant for the radar investigated in this thesis. [10]

One fundamental property of radar signals is the Doppler shift, where targets that move radially to a radar cause a change in received frequency, this shift is typically small compared to the radar's operating frequency. Doppler shift can be used to calculate radial velocity of the moving target. Following equation can be used to approximate Doppler shift with very high accuracy.

$$f_{\mathrm{d}} = \frac{2v_{\mathrm{r}}}{\mathrm{c}} f = \frac{2v_{\mathrm{r}}}{\lambda} \tag{9}$$

where f_{d} is the amount of frequency shift, v_{r} is target's radial speed, positive value means approaching target and negative value means receding target. c is speed of light, f stands for transmitted frequency and λ stands for transmitted wavelength. [11]

Something that all radars also have in common is clutter. Clutter in terms of radars is anything that is of no interest to the on-going task. In an example, one radar might try to track airplanes and detect clouds as clutter, while another radar that is used for meteorological surveillance, detects an airplane and it is considered as clutter. Usually clutter is nature, like vegetation, sea, rocks and other not wanted objects that get detected by radar. Nowadays one major source of clutter are the windmills used for energy production. Clutter is inevitable in most use cases, because just like the objects that we want to detect, also other objects reflect electromagnetic waves back to the radar. [11]

Unlike noise, clutter does not have set power level where it appears, clutter has different signal-to-noise ratios (SNR) that can differ depending on factors like wind, which can increase or decrease clutter's SNR. Wind can result in clutter having many Doppler velocities, which makes it harder to filter out clutter. Clutter can be handled with filtering. A simple way to employ Doppler filtering is to remove clutter echoes that have an absolute radial velocity lower than a set threshold. [11]

Radar range equation and thermal noise equation can be used in combination to create SNR equation, which can be used to determine ratio of received signal power P_{R} to a noise power P_{N}. It is useful to estimate how much difference there is in these levels to determine how much headroom there is. [6]

$$\mathrm{SNR} = \frac{P_{\mathrm{T}} G_{\mathrm{T}} G_{\mathrm{R}} \lambda^2 \mathrm{RCS} G_{\mathrm{i}}}{(4\pi)^3 R^4 L_{\mathrm{a}} k T B_{\mathrm{N}} F_{\mathrm{n}}} \tag{10}$$

Integration gain G_{i} comes from taking multiple pulses of a signal and combining them to increase SNR. Combining these samples together will increase power level for correlated signal components. Noise is uncorrelated and by integrating over multiple pulses we will get average noise levels closer to 0, while echoes from a target are correlated and will have their power level unchanged. Integration gain is based on number of pulses used for integration. This means that by doubling our number of samples we also double SNR for those correlated signal components. [11]

2.1.3 Radar Modulation

The transmit signal introduced in equation (1) can be modulated to increase radar performance and capability. Modulations are widely used in radars and one of the most common type of modulation, also used in the radar investigated in this thesis, linear frequency modulation, is introduced more in detail.

Figure 1 shows five different signals, first is a carrier signal with no modulation, 2nd is baseband signal that is used to modulate other signals, so that beat signal can be read from a demodulated signal, 3rd is an amplitude modulated (AM), 4th is a frequency modulated (FM) signal and 5th is a phase modulated (PM) signal. We can see that with different modulation schemes, specific parameter of a signal will change in relation to the baseband signal. Amplitude modulation changes signal's amplitude, frequency modulation changes signal's frequency over time and phase modulation changes signal's phase. All of these signals can be used to carry the baseband signal, but modulation method is different, resulting in different waveforms. [4]

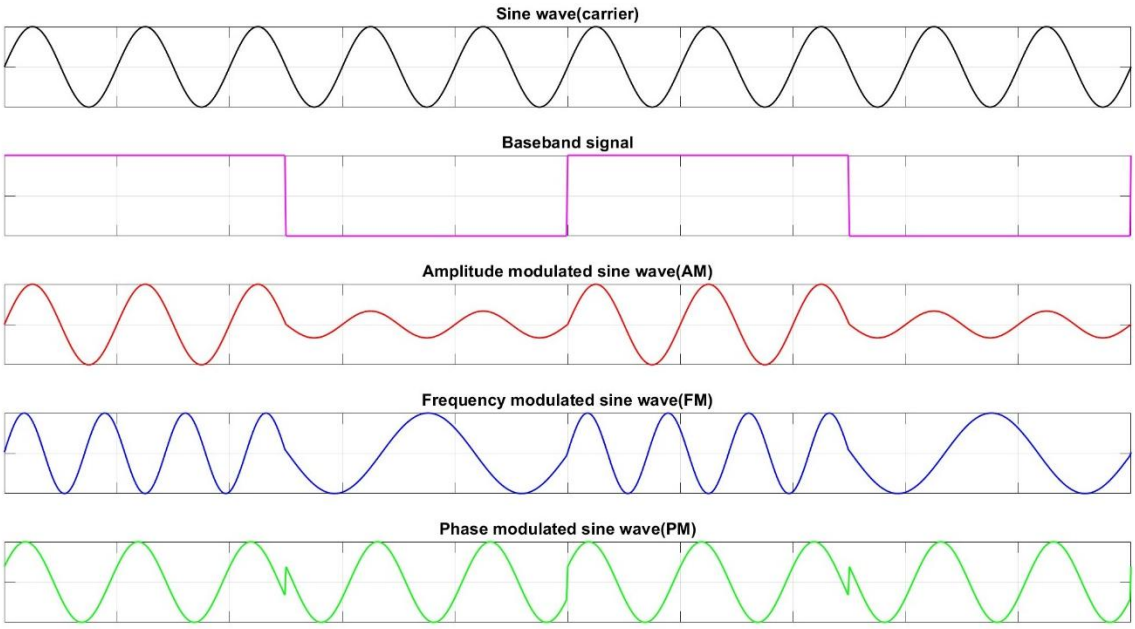

Figure 1: *Different modulations visualized*

Amplitude modulation can be expressed as:

$$\bar{x}(\mathrm{t}) = [A + m(t)]\cos(2\pi f_{\mathrm{c}} t) \tag{11}$$

Here A is our carrier amplitude before modulation and $m(t)$ is a signal used to modulate the transmitted waveform. Here $A + m(t)$ has replaced $a(t)$ in equation (1). Phase modulation can be expressed as:

$$\bar{x}(\mathrm{t}) = a(t)\cos(f_{\mathrm{c}} 2\pi t + k_{\mathrm{p}} m(t)) \tag{12}$$

Here k_{p} is phase modulation multiplier, which affects how much phase changes according to the message signal $m(t)$. To form a frequency modulated signal, we can take the signal model from equation (1) and make derivative of $\varphi(t)$ to be a transmit frequency $f(t) = \frac{d}{dt}\varphi(t)$. We can make amplitude term $a(t) = 1$, because we are not using amplitude modulation here. Next modulation method, frequency modulation can be represented as:

$$\bar{x}(\mathrm{t}) = \cos\left(f_{\mathrm{c}} 2\pi t + 2\pi k_{\mathrm{f}} \int_0^t m(t_{\mathrm{m}})\, dt_{\mathrm{m}}\right) \tag{13}$$

Here we have our frequency modulating part: $2\pi k_{\mathrm{f}} \int_0^t m(t_{\mathrm{m}})\, dt_{\mathrm{m}}$, where k_{f} is frequency modulation multiplier, which tells how much frequency changes. $m(t_{\mathrm{m}})$ is the message signal again, which changes signal frequency. [12]

One of the most common frequency modulation schemes used in a CW radar is linear frequency modulation. In this modulation method we start from carrier frequency f_c and change our transmit frequency over time. To form a modulated LFM signal, we need to form the frequency modulation f_{m}:

$$f_{\mathrm{m}}(t) = -\frac{B_{\mathrm{chirp}}}{2} + \frac{B_{\mathrm{chirp}}}{t_{\mathrm{chirp}}} * t, \qquad 0 \le t \le t_{\mathrm{chirp}} \tag{14}$$

This model represents one chirp and these chirps are constantly transmitted. With this applied to signal model in (13), it leads to a signal that is linear frequency modulated. B_{chirp} is the frequency change during one chirp and T_{chirp} is length of the chirp in time. Lastly t is instant time. This frequency modulation will then be substituted to k_{f} and the message signal $m(t_{\mathrm{m}})$.

$$\bar{x}(\mathrm{t}) = \cos\left(f_{\mathrm{c}} 2\pi t + 2\pi B_{\mathrm{chirp}} \int_0^t \left(-\frac{1}{2} + \frac{t}{t_{\mathrm{chirp}}}\right) dt\right), \qquad 0 \le t \le t_{\mathrm{chirp}} \tag{15}$$

We can now write the transmit signal as:

$$\bar{x}(\mathrm{t}) = \cos\left(f_{\mathrm{c}} 2\pi t + \pi B_{\mathrm{chirp}} t + \pi \frac{B_{\mathrm{chirp}}}{t_{\mathrm{chirp}}} * t^2\right), \qquad 0 \le t \le t_{\mathrm{chirp}} \tag{16}$$

This creates so called chirp signal, which is ascending. By inverting the modulation multiplier, we can change this chirp to be descending:

$$\bar{x}(\mathrm{t}) = \cos\left(f_{\mathrm{c}} 2\pi t - \pi B_{\mathrm{chirp}} t + \pi \frac{B_{\mathrm{chirp}}}{t_{\mathrm{chirp}}} * t^2\right), \qquad 0 \le t \le t_{\mathrm{chirp}} \tag{17}$$

All of these signal models create signal, which consists of one chirp with a length of t_{chirp}. In radar use, these chirps would be transmitted one after the other. We can simplify this modulated signal model by denoting frequency modulation as f_{m}:

$$\bar{x}(\mathrm{t}) = \cos\left(2\pi t[f_{\mathrm{c}} + f_{\mathrm{m}}(t)]\right) \tag{18}$$

Shown in Figure 2 is an example of ascending chirp. There on the horizontal axis we have transmitted frequency $f(t)$ and on the vertical axis we have time t. Here f_{B} is the beat frequency, which is difference in frequency between the transmitted and received signals. Then τ, which is propagation delay. Propagation delay and beat frequency are directly proportional. This is the time it takes for an echo from target p to return to the radar. Transmit frequency will fall back to the starting frequency f_{c} at the beginning of next chirp. This creates a sawtooth like image for the modulated signal in frequency time figure. [12]

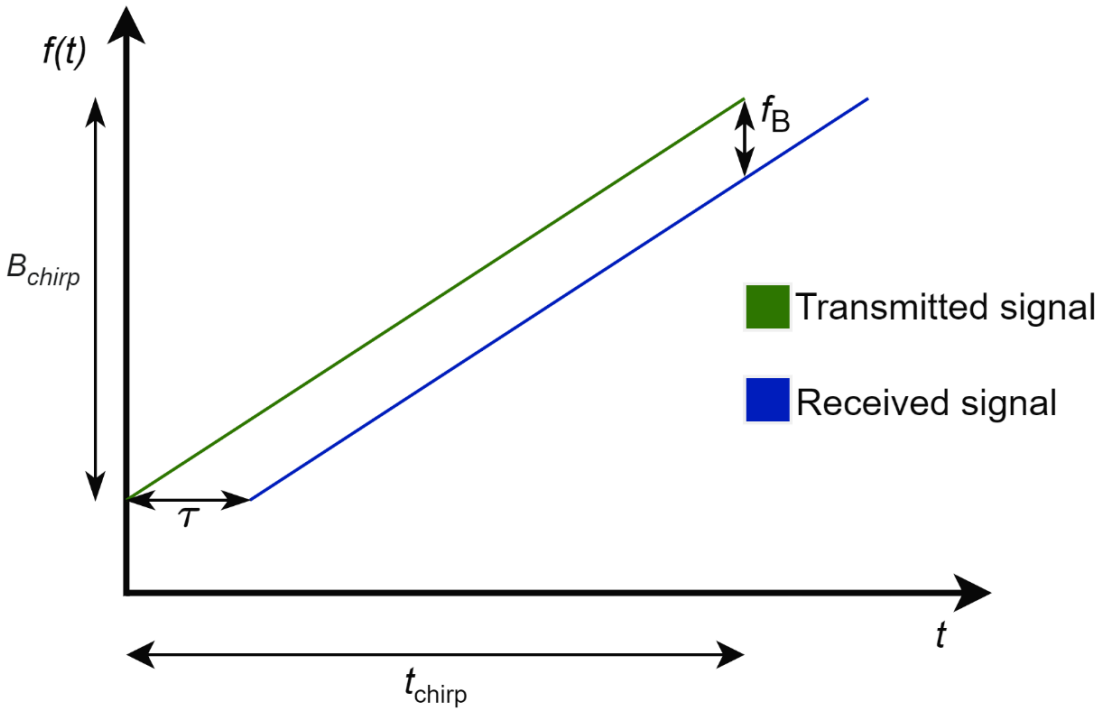

Figure 2: *LFM chirp*

Going back from modulation, we can denote a complex baseband signal with:

$$x(\mathrm{t}) = a(t)\mathrm{e}^{\mathrm{j}\varphi(t)} \tag{19}$$

this is what is left of a baseband signal after demodulation and is called the complex envelope of the waveform. [4]

Amplitude modulation is generally not used in radars, because it usually leads to lower transmitted signal amplitude and therefore transmitted energy, which will have a negative effect on the radar performance. We will not be focusing on AM because radar investigated in the thesis does not utilize it. [11]

Frequency modulation is widely used in radars, most used type is LFM, where transmitted frequency within a pulse linearly changes with time, this kind of signal with linear increase in frequency is usually referred to as a “chirp”, because in audible frequencies this kind of waveform produces a chirping sound. [11]

2.2 Pulse Radar

Pulse radar operates with the principle of sending radio frequency pulses one at a time. Pulse radars do this by using a switch that connects and disconnects TX and RX sides from the antenna element. Same antenna can be used for both, but the transmission and reception typically does not occur at the same time to avoid receiver saturation. This switching allows pulse radars to use higher transmit power, because receiver will not be disrupted by the high power. [13]

Pulse radars work periodically, pulse is sent, and after that radar is listening for that pulse to reflect back. After certain set time, this cycle will start again and transmitter sends another pulse. Distances can be then calculated from these incoming reflections.

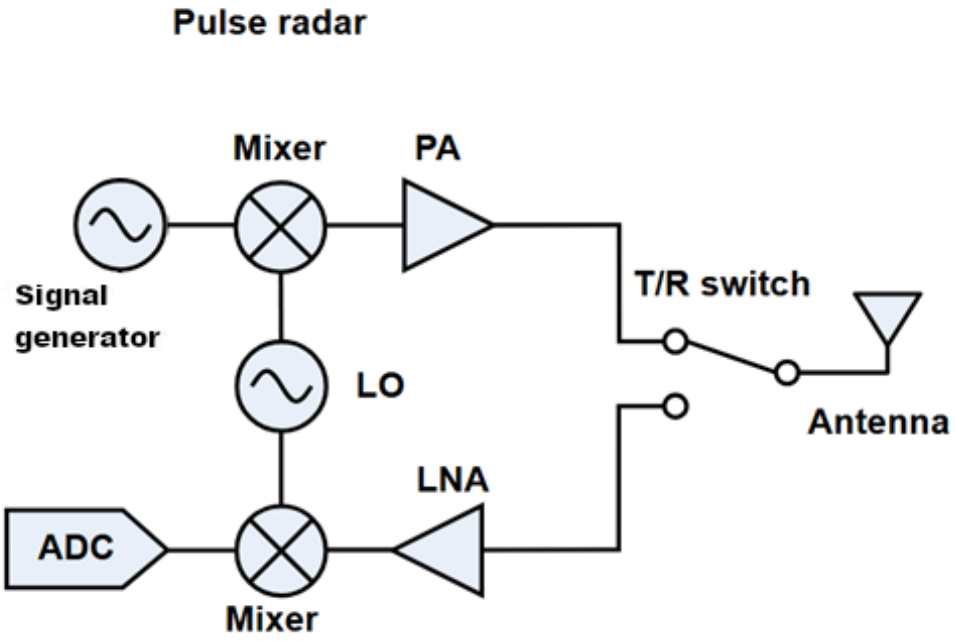

Figure 3: *Pulse radar block diagram* [14]

Simple pulse radar block diagram is shown in Figure 3. On top is transmitter side, which starts from signal generator. It can create modulated or unmodulated pulse, depending on the radar. From signal generator we get the baseband signal $x(t)$. After that we have mixer, which multiplies the pulse sweep with the carrier frequency f_c, that comes from local oscillator (LO) and makes the signal be on the carrier frequency, that is when the signal becomes $\bar{x}(t)$ as in equation (1). After that we have a power amplifier (PA), which amplifies the signal level. From there we have a transmitter/receiver (T/R) switch, which quickly switches between the transmitter and receiver sides. Then we have an antenna that is connected through T/R switch to either transmitter or receiver side of the radar. [11]

On the receiver side after the antenna and T/R switch we have a low noise amplifier (LNA) that amplifies the received signal. Received signal level is typically too low to accurately detect changes in it, so amplifier is used to boost these differences in the signal. It also amplifies noise that is introduced to the signal from the channel. LNA is used to minimize noise amplification inherent in power amplifiers. After that we have a mixer again, this time it is used to do down conversion, where we return the signal from carrier frequency back to baseband signal. That baseband signal is then captured by the analog-to-digital converter (ADC), which digitizes signal samples received by the radar. [11]

Pulse radars have specific parameters that affect pulse radar performance, while all formulas and phenomena covered earlier also apply here, but pulse radars have specific

constraints and limitations, which are necessary to understand in order to analyze their performance. These limitations are in place because of the switching between transmitting and receiving, this causes a situation where pulse radar is not able to receive signals all the time and therefore it is necessary to take this into account correctly when deciding specifications for a pulse radar. [13]

Frequency of detections for pulse radar is limited by radars pulse repetition frequency (PRF)

$$\mathrm{PRF} = \frac{1}{\mathrm{PRI}} \tag{20}$$

which is a parameter that tells how many pulses per second the radar transmits. Inverse of this is called pulse repetition interval (PRI), which is the time between two pulses, or total periodic time.

Maximum range of a radar defines PRF, because higher the pulse repetition frequency, the more often radar is able to gather information about surroundings, but pulse repetition frequency is limited by maximum range, because while electromagnetic waves travel at the speed of light, radar would still have to increase receiving time window, so that higher range echoes can reach back to the radar before we start new transmission. Echoes from high range can reach our radar during next receiving window. This leads to their range being estimated wrong, because our receiving window thinks that it is an echo from most recent transmission. This can be mitigated with long enough receiving window, waveform design or advanced processing. [13]

Pulse radars duty ratio tells how much time is taken by transmitting. Duty ratio can be calculated with following equation

$$\text{duty ratio} = \frac{\tau_\mathrm{t}}{\mathrm{PRI}} = \tau_\mathrm{t} * \mathrm{PRF} \tag{21}$$

where τ_t is transmit period. Basically, the lower duty ratio we have, the more time we are able to receive echoes back to radar and therefore, the better chance we have of detecting objects. Lower duty ratio means better performing radar in terms of detecting capability, but too short transmitting time means that we will not be able to transmit enough energy to make use of our receiving time, which can cause us to lose small targets at long ranges. This comes down to compromises and making sure specifications are in line of the mission that radar is needed for. [13]

Range resolution in pulse radars is one big concern when deciding how long of a pulse to use. There is only one variable that will affect the range resolution of pulse radar, which is pulse length in time. Pulse radar range resolution can be calculated with formula

$$\Delta R = \frac{c\tau_t}{2} \tag{22}$$

This is how range resolution is defined for a basic pulse radar. Shorter pulse time will make the range resolution smaller, which is better, but it is a trade-off between energy received and range resolution that needs to be made. Longer pulse increases received energy, which will increase maximum range and allow better SNR from targets with low RCS, but makes range resolution worse. [11]

Pulse radars require very high peak power, because transmitter is not constantly on and therefore, we have a lot of times when our transmitted power is 0, we can calculate our radar's average power with

$$P_{avg} = P_{pk} * \text{duty ratio} \tag{23}$$

where P_{avg} is our radars average power and P_{pk} is our peak power. This average power is the power that would be required to transmit continuously for same power levels. We need very high peak transmit power to achieve the same total transmit power that we could achieve a lot easier if we were to send it continuously. This means we will need to have hardware that can handle high transmit power for short periods of time, but we still have rather low average power. [13]

Pulse radars suffer from blind spots in range, due to the receiver being off during transmission + guard period. It follows, that there is minimum range for pulse radars, due to receiver not being on and also switching between transmitting and receiving takes time. Switching is very fast, usually measured in nanoseconds, but long enough to create a range that we cannot detect from because we do not have receiver ready for receiving echoes. Minimum range of pulse radar is given by

$$R_{min} = \frac{c(\tau_t + t_{tr})}{2} \tag{24}$$

where t_{tr} is switching time from transmit to receive. This minimum distance is a reason that pulse radar cannot be good for high range and low range applications at the same time, compromises result in the radar working well in only one or the other. Minimum range is illustrated in Figure 4. [13]

Figure 4: *Minimum range* [13]

Eclipsing is also an unavoidable downside of pulse radars, this occurs when we transitioning from receiving period back to transmitting period, received signal can be partially or fully lost because of transmission, and cannot be received and detected correctly. This phenomenon is called eclipsing and this blind range can affect a series of different ranges, where the distance between object and radar is just right so that electromagnetic wave round trip time matches our total periodic time, this means we always receive an echo back during our transmission. Partial eclipse is also bad and drastically lowers our received signal energy, which can make it harder to detect those objects. Changes in received energy cause by eclipsing is demonstrated in Figure 5. [13]

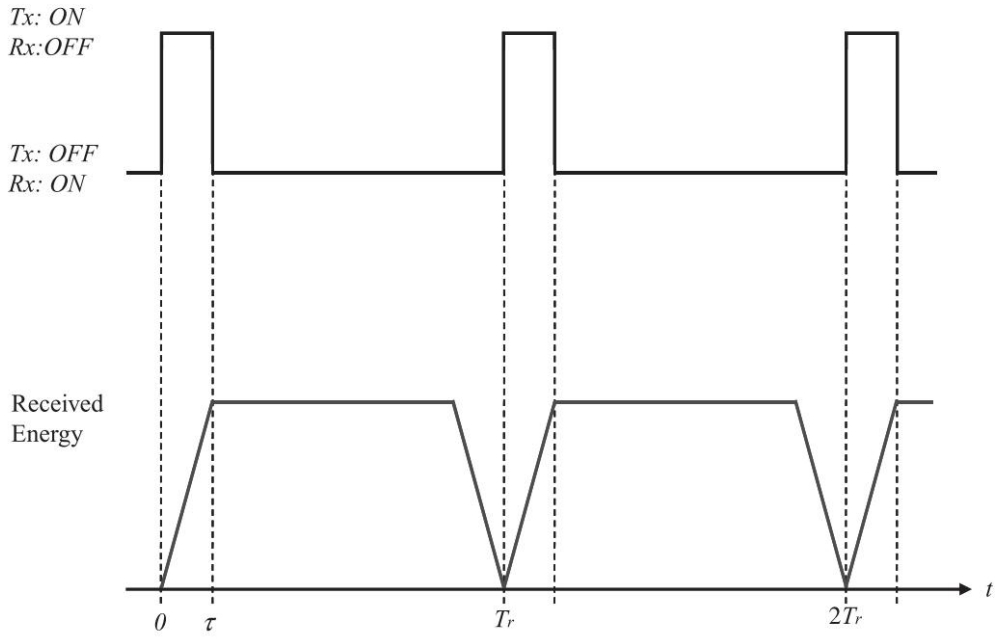

Figure 5: *Variation of received echo energy due to eclipsing* [13]

Pulse radars typically do range estimation by utilizing cross correlation between transmitted and received pulse. We can use the transmitted signal from equation (1) and received signal will be:

$$y(t) = x_p(t - \tau_p) + z_w(t) + z_i(t) \tag{25}$$

This received signal is delayed by propagation delay τ and has additional noise from the channel added to it. We can then do cross correlation between this and complex conjugate of the transmitted signal denoted as x^* to receive the baseband signal $y_{cc}(t)$:

$$y_{cc}(\tau) = \int_0^t x^*(t) y(t - \tau)\ dt \tag{26}$$

From cross correlation $y_{cc}(\tau)$ we can find the peak values that correspond to τ, which indicates the propagation delay τ that we can use to calculate range R by inserting it into equation:

$$R = \frac{c\tau}{2} \tag{27}$$

Pulse radars often use modulated signals to increase their performance, normal unmodulated pulse radar always has a trade-off between energy and range resolution, because longer pulse means worse range resolution and higher energy transmitted and vice versa, short pulse has good range resolution but low energy transmitted. This can be mitigated with use of modulated signals and is called pulse compression. Any modulation method can be used for pulse radars. [11]

Frequency modulation and phase modulation are popular modulation methods used for pulse radar. They enable the radar to keep transmitted energy high while having great range resolution. Modulated pulses mean that every point of the signal will be unique and each part of the signal can be distinguished when correlating with received signal. Modulation reduces the amount of sidelobes present in cross-correlation signal $y_{cc}(\tau)$, which means we will have better range resolution, because correlation between transmitted and received signals will have a clean single peak. [11]

Pulse radars are able to estimate Doppler shift caused by a moving object, which means we are able to estimate object's radial speed to the radar. We can achieve this by creating a time series with data from a series of pulses. Pulses will form a matrix with detection ranges on one axis and different pulses on the other axis, as shown in Figure 6.

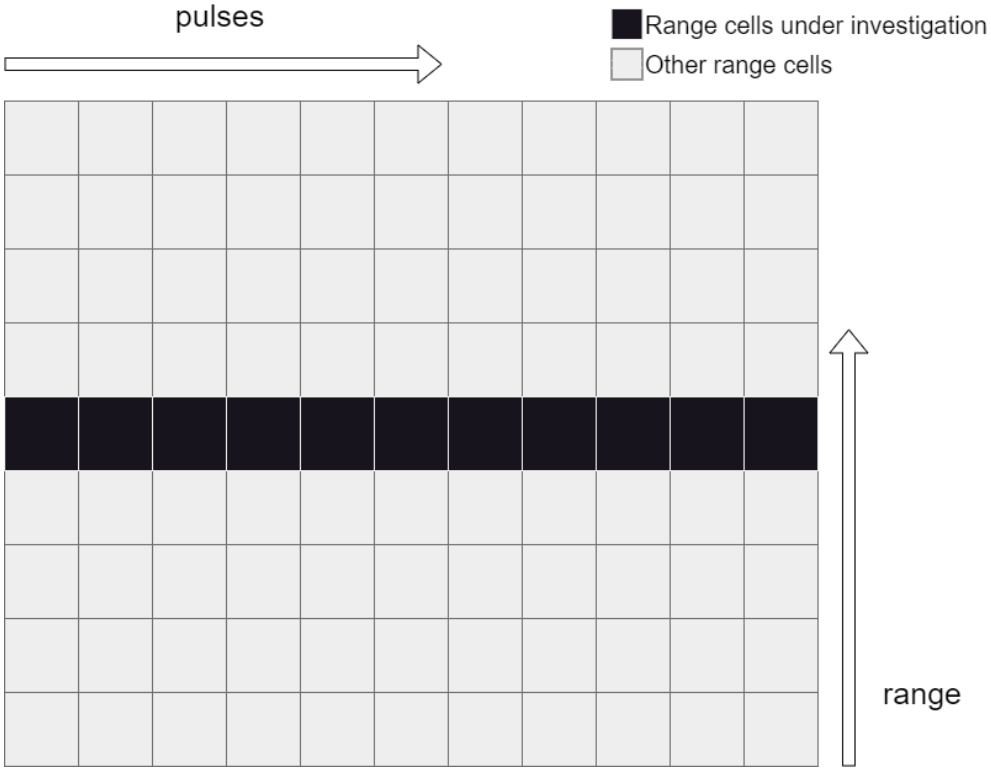

Figure 6: *Pulse/range matrix*

This matrix now has information of different range bins and pulses. Each cell contains one complex sample from the radar. Time between consecutive pulses is pulse repetition interval, which means shown in Figure 6 is actually fast/slow time figure, fast time dimension means range over one single pulse and slow time, which means dimension over multiple pulses. Complex samples in bins include information about received signals frequency, phase and amplitude. We can now apply fast Fourier transform (FFT) algorithm over slow-time. This then transforms the range/slow time figure to a range/Doppler frequency figure. This frequency data now directly corresponds to a Doppler shift and we can estimate Doppler shift from frequency data change between data samples. [11]

2.3 Continuous-Wave Radar

Continuous-wave (CW) radars do not use switching between transmitting and receiving like pulse radars do, instead as the name suggests, continuous-wave radars transmit constantly. To achieve this, CW radars typically use dedicated antennas for transmitting and receiving. It is possible to create CW radar that only uses one antenna with a circulator, which separates transmission energy from the received energy, but most CW radars use dedicated transmitter and receiver antennas, because common off-the-shelf circulators do not have high enough isolation to avoid disruptive levels of TX-to-RX leakage. [12][15]

Traditional CW radar transmits an unmodulated signal and are very limited in terms of measurement capability. Without any clear transmit and receive times CW radars cannot use a round trip time calculation to measure range like pulse radars can do. Unmodulated CW radars are not able to measure distance at all. Range measurement with CW requires frequency modulation or phase keying. These methods allow the radar to distinguish round trip time based on the change in the modulation that has been included in the transmitted signal. [15]

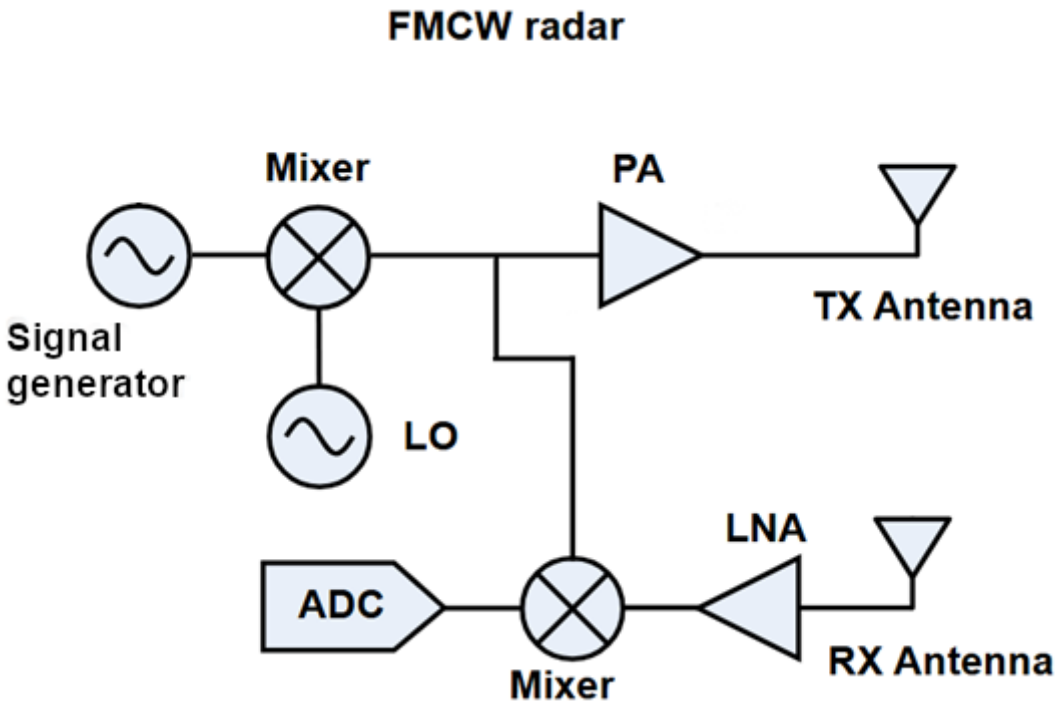

Figure 7: *FMCW radar block diagram* [14]

Simple FMCW radar block diagram is presented in Figure 7, this same block diagram can be used to describe CW radar also. Here transmitter side is on top and receiver side is on bottom. Transmitter side starts from sweep generator, which creates our baseband signal $x(t)$. This baseband signal is then mixed with carrier frequency f_c from LO. This creates our modulated transmit signal $\bar{x}(t)$. Then this signal is amplified with a PA to the desired transmit power. After that signal is transmitted using TX antenna. [15]

Receiver side starts from RX antenna, which captures the received signal $\bar{y}(t)$. This received signal is amplified using LNA to minimize noise added by the amplifier, while amplifying signal so that whole dynamic area of ADC can be utilized. From there this signal is mixed with the instant transmitted signal to convert it back to baseband signal $y(t)$. This baseband signal is then digitized using ADC. [15]

Regular CW radars are only used for detecting if object is moving, and if so, how fast the object is moving. Doppler shift plays a major role here, as discussed earlier Doppler shift

alters the frequency of the signal, but happens only with radial velocity. This means the placement for regular CW radars is crucial. They are commonly used for speed cameras on roads, because of cheap price and accurate measurement. This Doppler shift in terms of frequency is small relative to signal's carrier frequency, but it can be used to calculate objects speed. [16]

Doppler shift scales with used wavelength as seen in equation (10), this way we need to measure the relative shift when compared to our transmit frequency. This relative shift stays constant with objects that are moving at the same velocity, no matter what transmit frequency we use. With comparison of the received signal and the transmitted signal we can see how fast object is moving. We also can determine the direction, whether the object is moving towards the radar or away from the radar. [16]

Regular continuous-wave radar with unmodulated signal can only detect Doppler shift, which means that this type of radar cannot be used for ranging. For CW radars this can be solved by using modulation, which allows us to estimate range of detected object. [12]

Waveform design for CW radar focuses around frequency and phase modulation, and when looking at transmitted signal in equation (1), we see that term $\varphi(t)$ is the only one that we can modulate. Modulation of this term has to be continuous to keep our signal envelope constant to avoid interferences in frequency, when signal envelope is not continuous it will easily lead to these interferences. This can cause problems in signal processing, because signal cannot be interpreted correctly. For a LFMCW radar we can make our transmit signal to be (16). Transmit signal then looks like one in Figure 2. [12]

Now in ideal situation the received signal is a copy of the transmitted signal, but it is delayed by the propagation delay τ and frequency has shifted by the beat frequency f_{B}. However, in a real-world scenario received signal is sum of many delayed and frequency-shifted copies from all targets and leakage from TX to RX. Additional noise has also been introduced to the signal from channel:

$$\bar{y}(\mathrm{t}) = \sum_{p} a_p e^{j2\pi(t-\tau)\left[f_{\mathrm{c}}+f_{\mathrm{m}}+f_{\mathrm{B},p}+f_{\mathrm{d},p}\right]} + \mathrm{z}_{\mathrm{w}}(t) + \mathrm{z}_{\mathrm{i}}(t) \tag{28}$$

Here $\bar{y}(t)$ is the received signal, which is delayed and frequency-shifted version of the transmitted signal from all paths. The beat frequency f_{B} contains range and range-rate information in CW radars.

This received signal can then be dechirped by mixing it with copy of the transmit signal's complex conjugate:

$$y(\mathrm{t}) = \bar{y}(\mathrm{t})\bar{x}^{*}(\mathrm{t}) \tag{29}$$

From this the resulting signal is:

$$y(\mathrm{t}) = \sum_{p} a_p e^{j2\pi t\left[f_{\mathrm{B},p}+f_{\mathrm{d},p}\right]} + \mathrm{z_w}(t) + \mathrm{z_i}(t) \tag{30}$$

This is how we get the baseband signal and can extract the beat frequency from the received signal. Here the beat frequency consists of:

$$f_{\mathrm{B},p} = -f_{\mathrm{c}}\frac{2}{\mathrm{c}}v_{\mathrm{r},p} - \frac{B_{\mathrm{chirp}}}{t_{\mathrm{chirp}}}\frac{2}{\mathrm{c}}R_p \tag{31}$$

Here v_{r} is radiating object's radial velocity and distance to target R. From this we will use FFT to find beat signals for different echoes, which will be used to estimate target's range from the radar. We cannot calculate radial velocity directly from this, but we can use samples over multiple chirps to see the change in received signal phases, when we take FFT of this data over multiple received chirps, we are able to calculate target's radial velocity. [12]

There are constraints for this radar system in place, first we have beat frequency resolution, which can be calculated with:

$$\Delta f_{\mathrm{B}} = \frac{1}{t_{\mathrm{chirp}}} = \frac{B_{\mathrm{chirp}}}{t_{\mathrm{chirp}}}\frac{2}{c}\Delta R \tag{32}$$

Where we can calculate our range resolution to be:

$$\Delta R = \frac{c}{2 * B_{\mathrm{chirp}}} \tag{33}$$

This shows that range resolution depends on the chirp bandwidth, which has to be high enough to be able to accurately estimate target's range. Radial speed resolution then depends on how many samples we use to calculate with FFT. The more chirps we have, the more accurate results we can get for our radial speed. This resolution can be calculated with:

$$\Delta v_{\mathrm{r}} = \frac{\mathrm{c}}{2 * f_{\mathrm{c}}} * \frac{1}{t_{\mathrm{chirp}}} \tag{34}$$

We can see that radial speed resolution is dependent on the chirp duration. This is how continuous-wave radar can be used with modulation to make it also able to calculate range and not only Doppler shift caused by a target. [12]

2.4 Multiple-Input Multiple-Output Radar

Multiple-input multiple-output radar is a device that uses multiple antennas for transmission and reception. MIMO radar transmits independent waveforms from multiple transmit antennas. Receiver side of MIMO radar uses multiple antennas to receive back these independent signals reflected from the channel. Classification of MIMO radars is usually done in two main groups, this classification is done based on the spacing of the antennas. With antennas spaced closely together, we can assume that echoes from objects are most likely correlated between antennas. In a case where antennas are spaced further apart, we most likely have echoes coming to the antennas that are uncorrelated to each other and therefore they are categorized in their own class. This chapter will focus on radars that have antennas spaced closely together, so the ones that we can assume to have correlated echoes back from objects coming to the receiving antennas. [17]

Virtual antenna array is one special thing about MIMO radars, which improves angle resolution significantly. Usage of orthogonal waveforms allows us to form a virtual array of antennas, that is larger than our physical antenna array. This technique forms a unique pair from every transmitter-receiver combination, which allows us to have better angle resolution than our physical array allows. Number of antennas in our virtual array can be calculated with

$$N_{\mathrm{ant}} = N_{\mathrm{t}} * N_{\mathrm{r}} \tag{35}$$

where N_{ant} is the total amount of antennas that we have in our virtual array, N_{t} being the number of transmitters that we use to send orthogonal waveforms and N_{r} is the number of receivers receiving these orthogonal radiations. [17]

Configuring MIMO radar this way to transmit orthogonal waveforms from each transmit antenna allows our virtual antenna array to appear a lot bigger, for example if we have a radar with 4 transmit antennas and 8 receiving antennas, we have 12 physical antennas in total, but in terms of virtual antenna elements we have $4 * 8 = 32$ antenna elements in our virtual array. Larger virtual array improves radar angular resolution, since we have more unique antenna pairs that we can compare. Visual example of a MIMO radar with 2 transmit and 4 receiving antennas, which results in 8 virtual antennas is shown in Figure 8. [17]

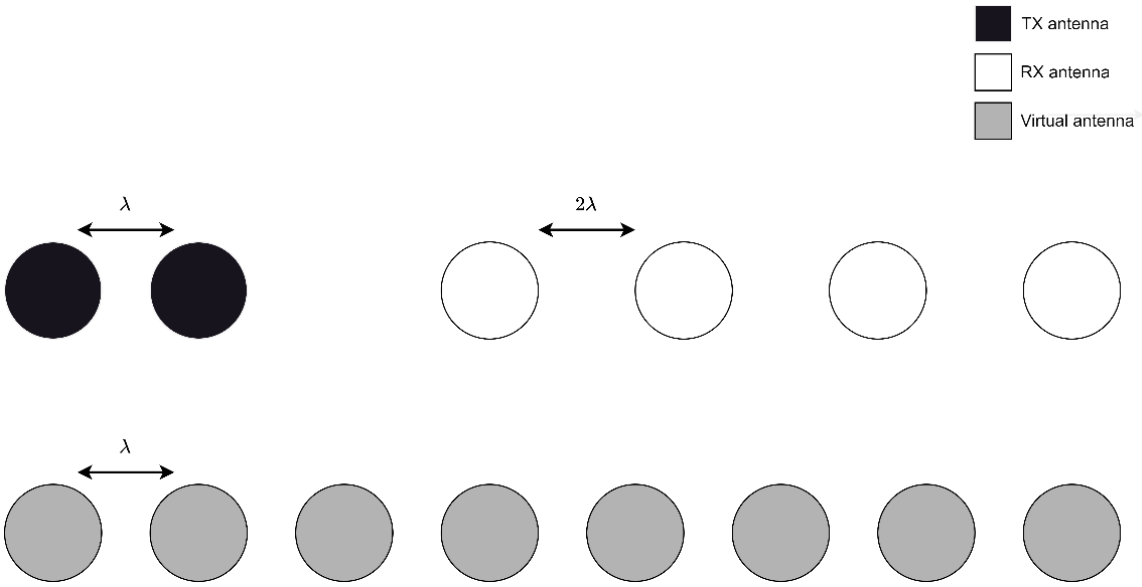

Figure 8: *MIMO TX, RX and virtual array* [19]

In Figure 8, TX antennas are separated with a distance of one wavelength and RX antennas are separated with a distance of two wavelengths. This results in a virtual array with spacing between elements being one wavelength. Placing of antenna elements matter, because it changes virtual antenna array and when placed incorrectly, virtual antennas will overlap and resulting virtual array does not get as large as it could. [18]

Location of virtual antenna elements can be calculated, for situation in Figure 8 we can say that our TX antennas are in locations $[0,\ \lambda]$ and our RX antennas are in locations $[0, 2\lambda, 4\lambda, 6\lambda]$. From this we can use equation:

$$l_{\mathrm{v}} = l_{\mathrm{t}} + l_{\mathrm{r}} \tag{36}$$

where l_{v} is location of the virtual antenna coming from TX antenna and RX antenna pair. l_{t} and l_{r} are locations of TX and RX antennas. For Figure 8 example we see that our first virtual antenna will be at location [0, 0] and last virtual antenna will be at location $[0,\ 7\lambda]$, which matches the figure. This can also be expanded to two-dimensional arrays, where same equation will work. This is illustrated in Figure 9.

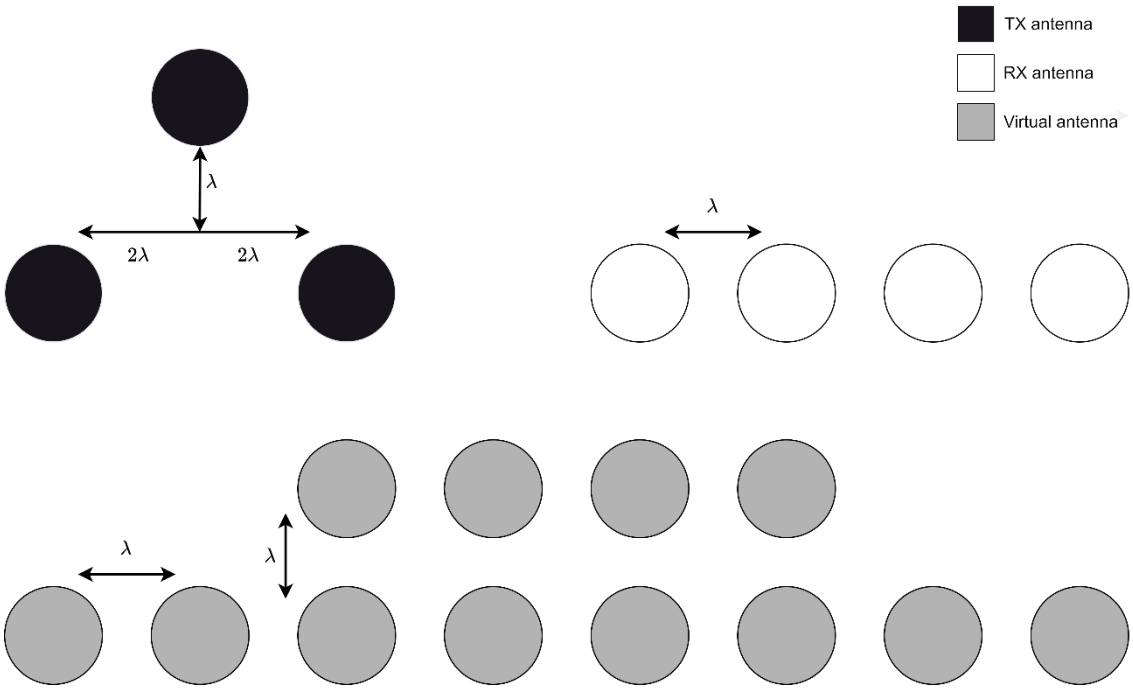

Figure 9: *Multidimensional MIMO array* [18]

In Figure 9 we can see how two-dimensional antenna placement results in a two-dimensional virtual array. With two-dimensional arrays we can use the same equation as in earlier example to calculate location of our virtual array elements. [18]

Let us use the example radar case with 4 transmit antennas and 8 receiving antennas, without utilizing orthogonal transmission and therefore larger virtual array, we would have only 8 different antennas that we can use to calculate angle from. This would work like multiple-input and single-output (MISO) radar then, but with MIMO technology we can utilize every receiving antenna once for every transmission antenna to determine the angle, this increases our angular resolution and therefore it makes MIMO radars more accurate in terms of angular performance. This orthogonal transmission can be achieved with time-division multiplexing (TDM) or frequency-division multiplexing (FDM). As names suggest, in TDM signal waves are timed so that waves will be orthogonal and with FDM frequency and therefore phase is shifted so that orthogonality is achieved. [17]

MIMO radars are able to calculate angle of arrival for signals that are received. This can be done by comparing phase shift between two or more receiving antennas. Phase shift to next antenna element can be calculated with:

$$\Phi_n = \frac{2\pi * n * d_{\text{ant}} * \sin\theta}{\lambda} \tag{37}$$

Here n is number of how many elements apart two antenna elements are from each other, d_{ant} is distance between two antenna elements and θ is the angle of arriving signal. This equation can be used to calculate phase shift between any two antenna elements. Difference between two neighbouring antenna elements should stay constant and average of more than two can be used to estimate angle of arrival, that way we have more points of reference for our angle estimation. This can be done with all receiving antennas and with MIMO antennas we can use our entire virtual antenna array for more reference points. More reference points are used to make the angle estimation more accurate. [19]

In equation (38) we can see that by calculating the phase shift between received signals from two antennas we can calculate the angle of arrival for the received signal between any two antenna elements by changing our equation to:

$$\theta_n = \arcsin\left(\frac{\Phi_n \lambda}{2\pi * n * d_{\text{ant}}}\right) \tag{38}$$

This tells us the azimuth direction of detected object. Same logic applies here as with phase shift calculations that more reference points will result to more accurate angle estimation, which is why we utilize MIMO virtual antenna array capability to improve our angle resolution performance. Using this to compute angle of arrival is very sensitive about receiver antenna spacing however, because when we have $d_{\text{ant}} > \lambda/2$ the periodical property of the equation results to lower accuracy, that is why usually $d_{\text{ant}} \leq \lambda/2$ is preferred for better accuracy. [19]

Spacing between antenna elements affects field of view (FOV) of a radar. From equation (37) we can see that angle of arrival is a periodic equation and we can estimate phase shift between antenna elements only in range of $(-\pi,\ \pi)$. We can substitute the phase difference Φ_n with a π to get equation for FOV:

$$\theta_{\text{FOV}} = \pm\arcsin\left(\frac{\lambda}{2 * n * d_{\text{ant}}}\right) \tag{39}$$

From this equation we can see that with antenna spacing of $d_{\text{ant}} = \lambda/2$ we can get our maximum FOV to be $\theta_{\text{FOV}} = \pm 90°$. [18]

Many algorithms have been created for angle of arrival estimation. Different kinds of antenna placements require different calculation algorithms. Estimator algorithms like MUSIC and ESPRIT are suitable for any kind of antenna array, whereas most FFT based angle estimation methods require a uniform antenna spacing, or virtual antenna array has to map uniformly. [20]

MIMO radars can use FFT based angle estimation, where incoming signals are sampled for each receiving antenna. These signals are then used to create so called ”angle FFT”, which results in us seeing a phase shift between each incoming signal. Virtual array is included in this, because each RX antenna will receive a signal transmitted from each TX antenna. This FFT data then has higher amplitude for frequencies, that had this frequency shift between antennas. This results in better angular resolution with more antenna elements, either physical or virtual, because the FFT will have more points for data and steps between these points are smaller. [18]

This FFT based approach also means that distinguishing between two different objects can be difficult. There needs to be enough phase shift for them to be distinguished in FFT. Required phase shift for two objects is:

$$\Delta\Phi > \left(\frac{2\pi}{N_{\text{ant}}}\right) \tag{40}$$

We see that our number of antennas N_{ant} affects our angle resolution significantly, by increasing number of antennas N_{ant} in our radar we can improve our angle resolution, which also means we are able to distinguish two objects that are close to each other in angle dimension. We can change this equation to see required angle of arrival θ difference between two objects:

$$\Delta\theta > \left(\frac{\lambda}{N_{\text{ant}} * d_{\text{ant}} * \cos(\theta)}\right) \tag{41}$$

here $\Delta\theta$ is angle between two different targets and we can see that because of cosine term we cannot distinguish two targets as close to each other when angle of approach increases. Because of this usually resolution is quoted for boresight view $\theta = 0$ and with assumption that antenna spacing $d_{\text{ant}} = \lambda/2$. This results in:

$$\theta_{\text{RES}} = \left(\frac{2}{N_{\text{ant}}}\right) \tag{42}$$

This is how we can describe angle resolution of a radar when using FFT based angle estimation. [18]

Radar only needs to distinguish two objects in one dimension, usually range or Doppler dimensions are used for this, because distinguishing in angle dimension requires very high antenna count to get high enough angle resolution. We are able to improve our results from this regular FFT approach by utilizing interpolation. This means we estimate angle of arrival between our points in FFT data. One method of this is shown below. [20]

To do this we first start with our angle FFT, where we take a number of M samples from signal $y[m]$, which are digitized signal samples from antennas and we get N-point FFT to be:

$$Y[i] = \left(\frac{2}{N_{\text{ant}}}\right) \sum_{m=0}^{M-1} y[m] e^{-j2\pi \frac{mi}{M}} \tag{43}$$

Here $y[m]$ is sample m from received signal y. We also have total number of samples used for FFT M. From this FFT data we can take our i -value that results in highest peak in FFT data. This is done over all range and Doppler dimensions elements. We are able to calculate then our estimated angle of arrival based on that information. Using our angle of arrival equation (38) we can map our FFT bin to an angle with:

$$\sin(\theta_{EST}) = \frac{i_{\max} - \frac{N_{\text{ant}}}{2}}{N_{\text{ant}}} * \frac{\lambda}{d_{\text{ant}}} \tag{44}$$

Here we first have to center our bins around 0 angle, we do that by subtracting $\frac{N_{\text{ant}}}{2}$ from our index $i_{\max}$. After this our resulting frequencies shift from $(0,\ 2\pi)$ to $(-\pi,\ \pi)$. By doing this we can then calculate our signals angle of arrival and angles associated with our FFT data points will be correct. [11]

One way to interpolate this data is to fit a polynomial through our FFT peak and neighbouring points. Resulting k index change from this can be calculated with:

$$\Delta \text{i} = -\frac{1}{2} \frac{\{|Y[i_{\max}+1]| - |Y[i_{\max}-1]|\}}{\left||Y[i_{\max}-1]| - 2|Y[i_{\max}]| + |Y[i_{\max}+1]|\right|} \tag{45}$$

Which we can then change in our angle estimation equation to make it:

$$\sin(\theta_{\text{EST}}) = \frac{(i_{\max} + \Delta \text{i}) - \frac{N_{\text{ant}}}{2}}{N_{\text{ant}}} * \frac{\lambda}{d_{\text{ant}}} \tag{46}$$

Now this equation results in more accurate angle estimation and improves our angle accuracy beyond given resolution. This can be utilized in other dimensions as well for more accurate range and Doppler estimation. [11]

2.5 Radar Detection and CFAR

Radar's ability to detect object relies on high enough SNR. However, with clutter or interference we need high enough signal-to-clutter ratio (SCR) or signal-to-interference ratio (SIR). These clutters and interferences can be seen as false detections, and therefore we have to filter these out to minimize false detections. This can be achieved by setting a threshold that will filter out all detections, which have their SNR level under this threshold. There's one very big downside to this, because it is very easy to miss out actual detections with this hard threshold set in place. Especially when range increases, we will naturally lose a lot of SNR from our object detections and these will especially suffer from one global threshold. [21]

One very useful algorithm for this problem is constant false alarm rate (CFAR) algorithm. CFAR algorithms are designed to track changes in incoming signals. CFAR algorithm checks changes in interference and clutter to change detection thresholds so that false detections will be kept constant while keeping the detection probability high for real targets. There are many different CFAR algorithms with different advantages and disadvantages. [4]

CFAR algorithm uses neighbouring range and Doppler cells to estimate the local noise power, this local noise level can adapt to local levels of clutter and interference related noise. This way we do not need to use one set threshold to filter across all ranges, but rather use local levels to estimate good filtering level for each area. Areas with high clutter and interference will still make it hard to detect our object in these areas, but it will only have a local effect and not global, like it would if we were to filter it out with global threshold filter. With this kind of local filtering, we are able to limit our false detections to constant rate. Algorithms like this are used widely in modern radars. [21]

CFAR algorithms use digitized samples from ADC. Simplest CFAR algorithm is CA (Cell Average)-CFAR, which is used in radar investigated in this thesis. CA-CFAR works with reference windows as illustrated in Figure 10 and Figure 11.

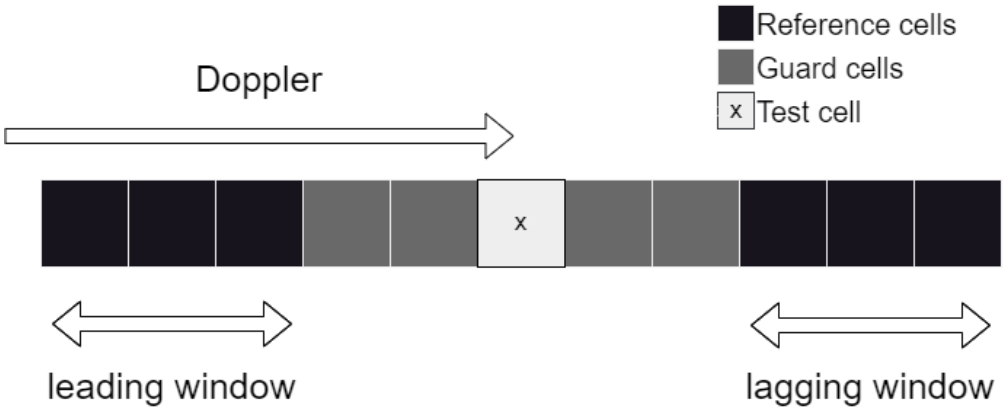

Figure 10: *One-dimensional window for Doppler processing*

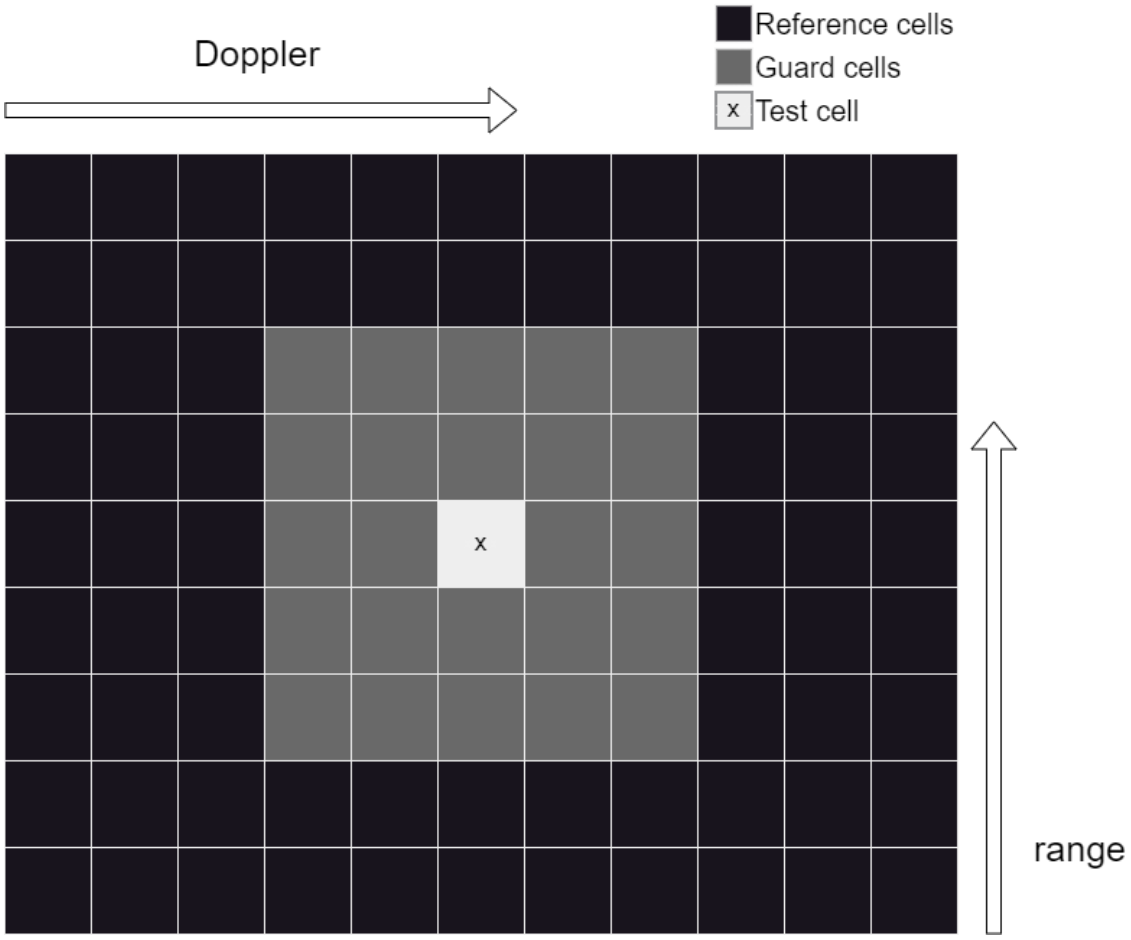

Figure 11: *Two-dimensional window for Doppler-range processing*

Figure 10 shows one-dimensional array with the test cell being in the middle, that is the cell for which we are determining the presence of a target. Around the test cell in grey are guard cells, which we are using only as a buffer around the test cell, because a strong target from the test cell might leak power to these neighbouring cells and increase the threshold counterproductively. Around guard cells there are reference cells, which are then used to calculate our reference noise level. These can be split in leading and lagging windows, leading window is window before the test cell and lagging window is window after the test cell in the chosen dimension. All of these different types of cells together are referred to as the CFAR window. [4]

Figure 11 shows two-dimensional array with same colouring for cells as in Figure 10. In Figure 11 we have also taken range dimension into account and therefore increased the number of reference cells significantly. This means we have a lot more reference points, which can result in more accurate estimation for threshold, but also increases memory requirement significantly.

CA-CFAR calculates average power level from all reference cells, which is then used as a threshold for a detection in test cell. This works very well when there are no powerful targets or clutter in those reference cells. Powerful targets in reference window can raise the threshold too high and that can mean we might miss a detection in the test cell. This is especially bad in environments with a lot of large objects like buildings, which may cause a blind spot around them. This can also happen if we do not have sufficient number of guard cells and our strong target leaks power to reference cells. Situation where leaking power from a target causes the threshold to raise too high for a detection is called self-masking. This CFAR algorithm has limitations for it to work properly, targets should be separated so that they are never in a reference window at the same time, because it can cause them both to not be detected. Reference window should be homogenous, which means that clutter should be similar through the whole reference window. This means we should not have strong targets in the reference window. [4]

CA-CFAR is a local threshold equation:

$$H = a_{\mathrm{th}} * P_{\mathrm{N}} \tag{47}$$

Here threshold H is locally applied based on scaling factor a_{th} and estimated noise power P_{N}. Scaling factor is set to keep false alarm rate constant and it can be changed to allow for higher or lower false alarm rate. Estimated noise power P_{N} is calculated by:

$$P_{\mathrm{N}} = \frac{1}{N_{\mathrm{T}}} \sum_{m=1}^{N_{\mathrm{T}}} x_m \tag{48}$$

Here N_{T} is number of training cell used and x_{m} is signal power in each of these training cells. This then gives average signal power in each training cell, which will be used to estimate local noise power. [4]

Limitations in CA-CFAR have led to a need of different CFAR algorithms to combat these limitations. Few common algorithms are smallest-of cell-averaging CFAR (SOCA) and greater-of cell-averaging CFAR (GOCA). These algorithms work with same CFAR window that has reference and guard cells around the test cell. Difference between CA-CFAR and these two is that CA-CFAR utilizes all reference cells to calculate one average that is used as a detection threshold, whereas SOCA and GOCA split that window in two different parts, it can be done among any dimension that CFAR is utilized on. With these CFAR algorithms we calculate average noise power P_{N} for leading and lagging windows separately, and based on algorithm used, we either select our detection threshold to be lower or higher of those two. With SOCA algorithm we select smaller of these two averages to be the detection threshold. This helps especially with problems that big objects can cause by not including them in the threshold calculation, but it increases false detections around clutter. GOCA on the other hand decreases these detections around clutter edges, but it will also decrease probability to detect targets of interest around powerful objects. [4]

Processing can be brought even further by analysing data between detections. From these we can estimate targets path and location by utilizing a so-called tracker. Trackers gather information from radar detections and from there they can estimate where target is heading based on information gathered. The topic of trackers is out of scope for this Thesis, but it is good to know that this detection processing does not stop here and can be developed even further. [22]

3. RADAR CHARACTERIZATION

Main subject of this thesis is radar characterization, which is the act of analysing the performance of the radar. In this thesis we will be mostly concerned about radar performance and data analysis, but characterization can also include many different aspects like signal analysis, where the focus is on investigating how different signal parameters affect the results. Radar performance will be all about how well can we detect and distinguish a known object. We can calculate how well the radar should be able to theoretically detect objects with different RCS. This can be done with radar specifications and substituting them into a formula, but we also need to see if our real-world findings are in line with these theoretical maximums and calculations, because in a real-world scenario there are a lot of different aspects that affect the test results and things that feel insignificant can have a huge effect on the results. That is why radars need to be thoroughly tested and characterized to make sure that the performance matches our expectations.

Radar characterization services can be purchased as a service from companies like Novelic. These services from Novelic include different types of testing services, which can be done embedded on radar's electronics or for full system testing an anechoic chamber or field testing can be utilized. [3]

Embedded testing includes all electrical boards and their functionality, in terms of coefficients and powers. All different boards in a radar can be tested this way to gather data across the whole electronic system to see what restrictions the electronics have. [3]

Anechoic chamber can be utilized for radar characterization for controlled environment to test radar's transmit system without any external RF noise. This way only RF signal measured will be from the radar in question. This is great way to analyse radar characteristics such as field of view, range and receiver sensitivity. [3]

Last characterization service offered by Novelic is field testing, which can be utilized to see how radar works in the intended use case, with real targets or components which can mimic intended targets very closely. Field testing offers capability for a wide range of performance testing. These can include but are not limited to analysing field of view, accuracy in that field of view, maximum range and separation between two or more targets. [3]

Parameter:	**Symbol:**	**Value:**
Frequency	f_c	17 GHz
Wavelength	λ	0.0176 m
Bandwidth	B	Changeable
Number of transmitters	N_t	Multiple
Number of receivers	N_r	Multiple
Transmitter gain	G_T	$5\text{dBi} \approx 3.16$
Receiver gain	G_R	$5\text{dBi} \approx 3.16$
Power	P_{avg}	Estimated: 10.07 W
Noise factor	F_n	$3\ \text{dB} \approx 2$
Additional losses	L_a	Estimated $3\ \text{dB} \approx 2$
Chirp length	t_{chirp}	Changeable
Number of transmitted chirps	N_{chirp}	Changeable
Detection threshold	SNR_{th}	$15\ \text{dB}$
Modulation	–	LFM (ascending)
Radar type	–	FMCW

Table 1: *Radar's specifications used for characterization*

The FMCW-MIMO-radar characterized in this thesis has parameters shown in Table 1. The radar has many changeable parameters, which gives freedom for testing and allows different modes to be tested with the radar.

Transmit power of the radar could not be accurately measured due to limitations in radar and measurement equipment, however, estimations have been made that transmit power should be around 10 W. Noise factor is not sure either, but component listing and calculations lead to an estimate of 3 dB, which is our best guess and will be used for calculations. This noise factor mostly comes from amplifiers in the radar. Additional losses L_{a} come from feedlines to TX antennas and they are estimated to be 3 dB, this value will be used for calculation.

Electronic devices can have problems with higher temperatures. High temperatures can result in overheating. This is first thing to test, because then we can know how the radar's temperature affects our measurement results. Temperature behaviour was measured in an over-the-air (OTA) chamber with receiving antenna directly in front of the radar. Parameters used in this measurement were set so that overheating can be achieved and power measurements are not absolutely correct, but relative difference should apply to other parameter modes as well, so we can use relative differences measured to correct the calculations.

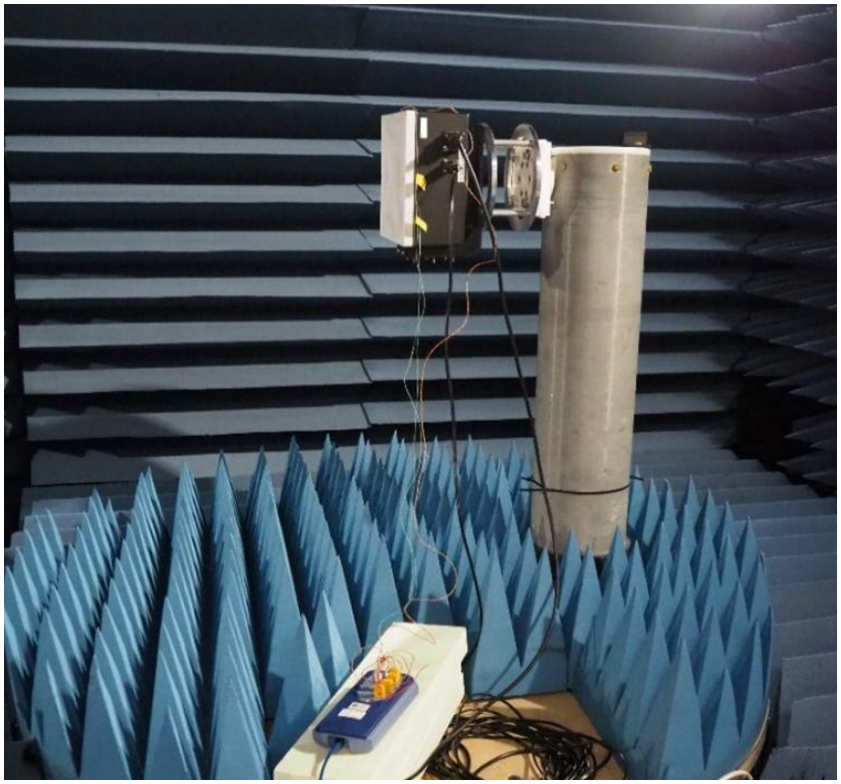

Figure 12: *Radar in the OTA chamber*

Test setup in Figure 12 was fitted with additional temperature sensors to verify that the internal temperature sensor is correct. One of these, which is physically closest to the internal temperature sensor will be plotted alongside the internal temperature sensor data to verify that they are matching.

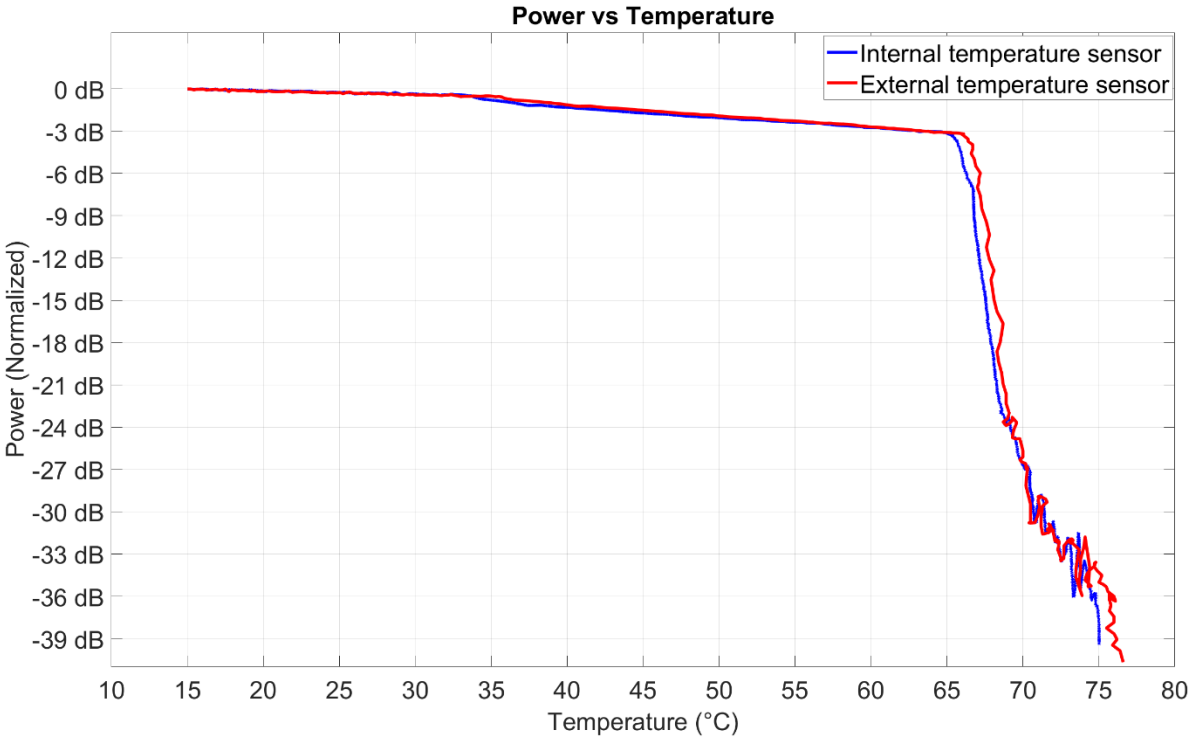

Figure 13: *Transmit power vs Temperature results*

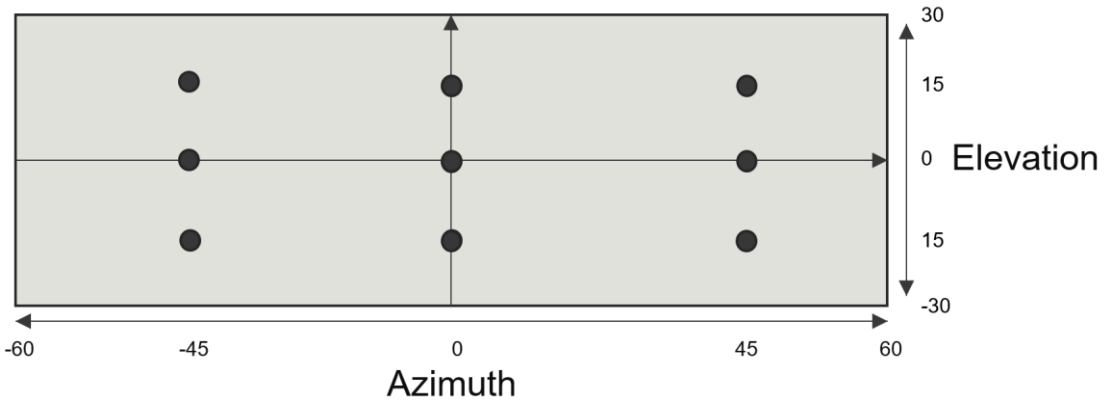

Figure 14: *Antenna pattern measurement locations*

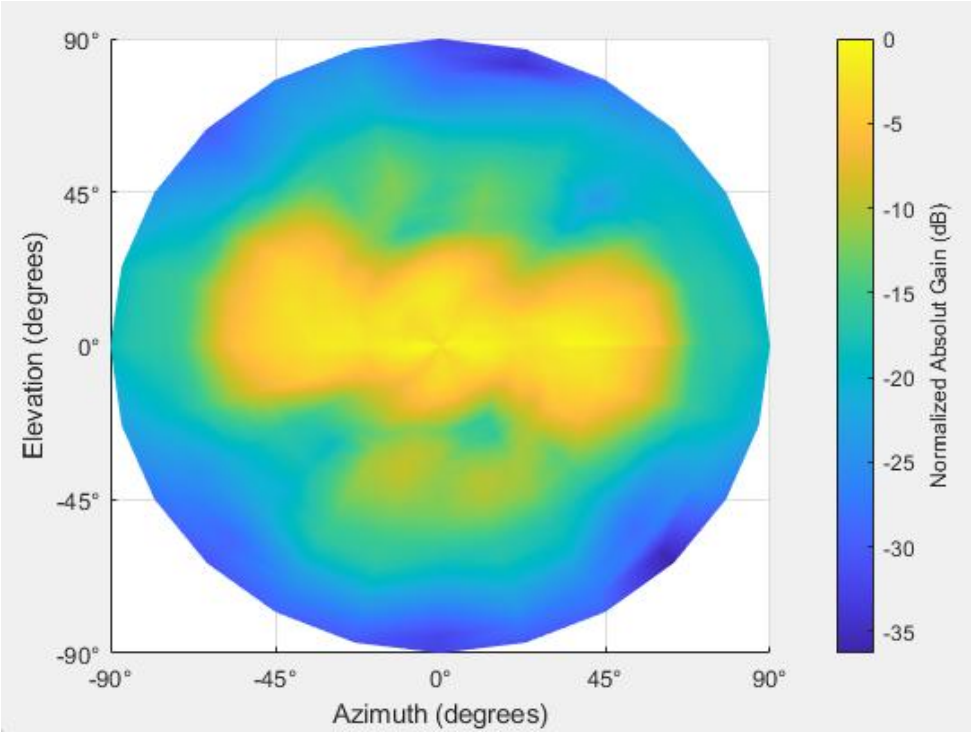

Figure 15: *Radar's antenna pattern result*

From Figure 13 we can see that temperature where the radar transmit power is $3\,\mathrm{dB}$ lower from our maximum is around $65\,^{\circ}\mathrm{C}$. This data will be used as a parameter for thermal loss L_{t}.

During this measurement the radar's transmit antenna pattern was also measured. This way antenna pattern was able to be visualized for this thesis. Radar antenna pattern was measured from 9 different locations as shown in Figure 14.

During this measurement the radar's bearing and tilt was manually changed by rotating radar around so that antenna was directly pointing at different points, some of which are visualized in Figure 14. Receiving antenna was in point (0, 0). Power measurement data from these different measurements was then added together and normalized to form the antenna pattern graph shown in Figure 15.

From this we can see that our antenna pattern stays within 3 dB from the maximum from around -10° to 10° in elevation direction and -60° to 60° in azimuth direction. Characterization tests on the field will be done as close to the beam centre as possible to not introduce any additional losses from the antenna pattern. This result also shows that we have some playroom, and target does not have to be directly in centre of the transmit beam.

Before any more testing, there is a need to calibrate the radar received power, which comes out of the ADC. The radar's FFT data is mean of voltages at a specific frequency,

but it is changed to dB for simpler usage. This will be needed to estimate RCS of objects from the radar's FFT data. This will be done by measuring corner reflectors with known RCS values. Radar's FFT data will be captured and corner reflector will be set to a known distance for R. Thermal loss L_t will be checked from Figure 13 according to the radar's temperature sensor reading. This will be done using multiple sized corner reflectors to get enough results. setup is shown in Figure 16.

Figure 16: *Corner reflector test setup*

Corner reflector was hanging in the air with strings attached to it. Masts were used to prop the corner reflector as high as possible. Here R to our corner reflector is changing from 9 m to 11.5 m. This test is done for 3 different corner reflectors with different RCS values. Radar was positioned so that it was straight in front of the corner reflector.

This test will focus on verifying radar data using targets with known RCS values. Shown in Figure 16 is test setup used for these tests. In these tests 3 different sized corner reflectors were used with RCS of $0.5\ \mathrm{m}^2$, $0.2\ \mathrm{m}^2$ and $0.01\ \mathrm{m}^2$. Distance from radar to corner reflectors was in range of 9 m to 11.5 m. We start by finding out noise level from FFT data. Noise level is shown in Figure 17.

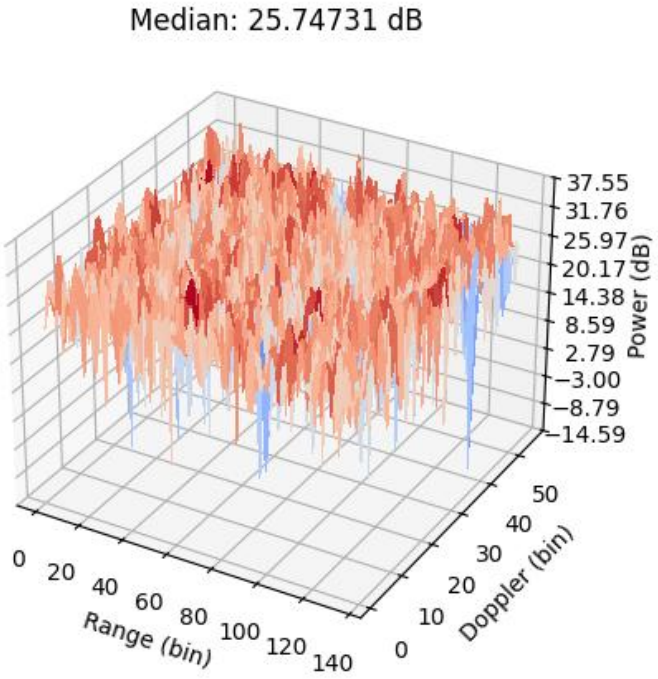

Figure 17: *Radar FFT data of thermal noise*

This data was taken from same data that corner reflectors were measured, here we can see that noise power stays at around 25 dB. We use this median value to normalize other measurement datas. This way we get SNR values for different corner reflectors, which can be utilized in upcoming field testing scenario. FFT data from measurements can be seen in Figures 18-20.

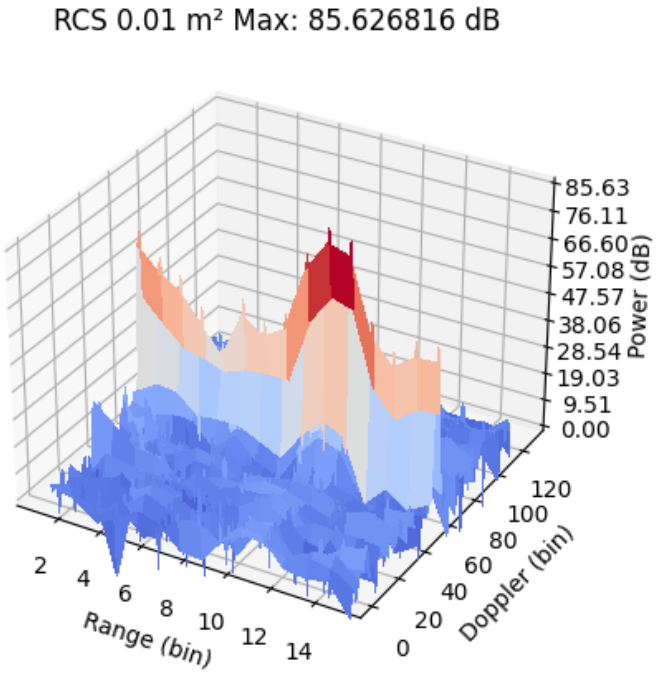

Figure 18: *FFT data from corner reflector with RCS of 0.01* m^2

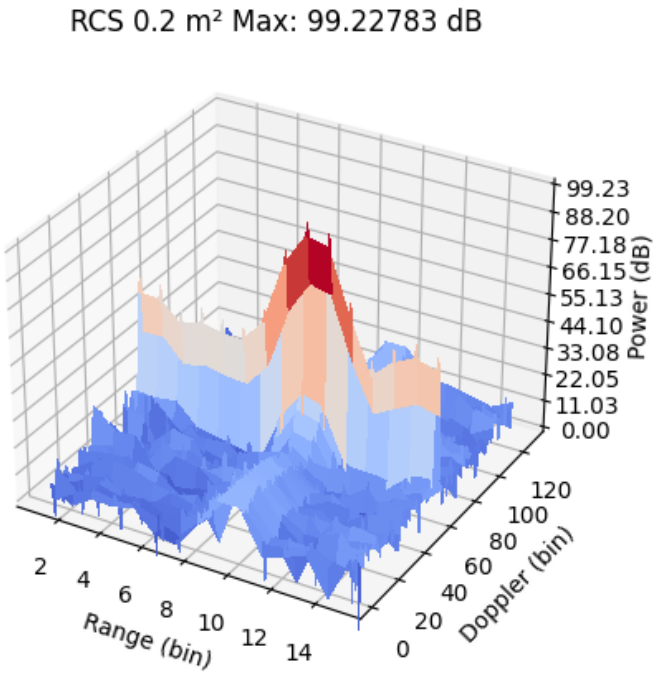

Figure 19: *FFT data from corner reflector with RCS of 0.2* m^2

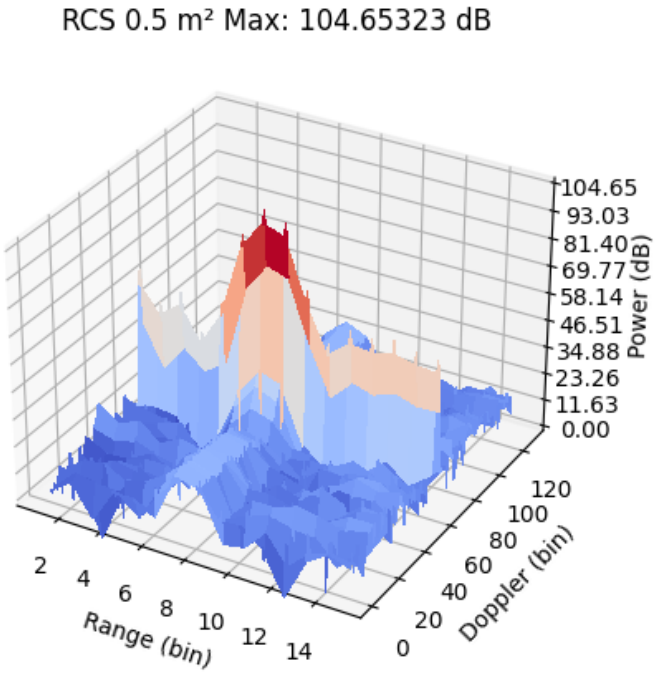

Figure 20: *FFT data from corner reflector with RCS of 0.5* m^2

R	RCS	SNR (dB)	T_R
9 m	$0.5\ \mathrm{m}^2$	104.65	$19\ °\mathrm{C} = 292.15\ \mathrm{K}$
10.7 m	$0.2\ \mathrm{m}^2$	99.23	$19\ °\mathrm{C} = 292.15\ \mathrm{K}$
11.5 m	$0.01\ \mathrm{m}^2$	85.63	$19\ °\mathrm{C} = 292.15\ \mathrm{K}$

Table 2: *RCS calibration measurement setups*

Shown in Table 2 are different test setups and resulting SNR values. T_R is temperature reading from the radar's temperature sensor, which read $19\ °\mathrm{C}$ during all tests, resulting in 0.04 dB from thermal losses, when compared to ideal temperature of $15\ °\mathrm{C}$. All of these tests were measured with integration time t_i of 25.6 ms.

From these values we can calculate theoretical difference in SNR that we should see as a result between different corner reflectors. In Table 3 these theoretical and real value differences are shown. Here theoretical values are normalized, with biggest of them being 0 dB.

R	RCS	SNR (dB)	P_{R} (dB) (Theoretical)
9 m	$0.5\ \mathrm{m}^2$	104.65	0
10.7 m	$0.2\ \mathrm{m}^2$	99.23 (-5.42)	-6.99
11.5 m	$0.01\ \mathrm{m}^2$	85.63 (-19.02)	-21.16

Table 3: *RCS calibration measurement results*

In Table 3 we can see that measured differences were different from theoretical ones, this can be because of many different reasons, which include not that accurate measurement of R and corner reflector might not be dead center in every measurement. Measurement setup was a bit flimsy and hard to control, so these are very realistic reasons for differences in the results. With these measured power levels, we are however able to estimate RCS of different targets and extrapolate how far we should be able to see a proper sized target.

4. FIELD TESTING SCENARIO

This chapter will focus on field test scenario, which focused on resolution's effect on the radar's performance. This chapter will include all relevant information on each test scenario and calculations will be done based on the results gathered.

After RCS scaling has been verified, next we test how different resolutions affect detection SNR. For this we need the radar's integration gain G_{i}, which is provided by equation:

$$G_{\mathrm{i}} = t_{\mathrm{i}} = \frac{N_{\mathrm{chirp}}}{B_{\mathrm{N}}} \tag{49}$$

We can see that integration gain can be calculated by solving integration time t_{i}, which is calculated by multiplying chirp duration t_{chirp} with number of chirps N_{chirp}. This then needs to be divided with noise bandwidth B. The radar utilizes integration to get better SNR from detections. This integration will be done over the whole integration time t_{i}. This means as long as our target stays in the same cell for the whole integration time we will have best integration gain. For this to happen the target needs to stay in the same range cell and the same Doppler cell throughout the whole integration time. Each range cell represents one ΔR that can be calculated by using equation (33), which means that too accurate range resolution can cause the target to not stay in single cell in the range dimension. This also applies to Doppler, where each cell represents one Δv_{r}, which for FMCW radar can be calculated by using modified version of equation (34):

$$\Delta v_{\mathrm{r}} = \frac{\mathrm{c}}{2 f_{\mathrm{c}} N_{\mathrm{chirp}} t_{\mathrm{chirp}}} \tag{50}$$

Too fine Doppler resolution can make the target to be in different cells over the integration time. With this in mind we need to add variables to equation (10). We replace integration gain G_{i} with the integration time t_{i} as seen from equation (49). We also need to add additional losses from the radar hardware L_{a} and temperature depending losses L_{T} so it becomes:

$$\mathrm{SNR} = \frac{P_{\mathrm{T}} G_{\mathrm{T}} G_{\mathrm{R}} \lambda^2 \mathrm{RCS}\, t_{\mathrm{i}}}{(4\pi)^3 R^4 L_{\mathrm{a}} k T F_{\mathrm{n}} L_{\mathrm{T}}} \tag{51}$$

Now we can substitute our known values and SNR equation becomes:

$$\mathrm{SNR} = \frac{1.95 * 10^{-7} P_{\mathrm{T}}\, \mathrm{RCS}\, t_{\mathrm{i}}}{R^4 k T L_{\mathrm{T}}} \tag{52}$$

Now we need to check temperature during measurements to calculate our estimated noise power kT and check detection SNR to verify that our power estimation is correct. Results from this drone testing can then be applied to equation (52) to verify that the estimations are correct. During this test different resolutions will be tested and SNRs from the detections will be investigated. This way we can see how different resolutions affect detection SNR. This testing will be done utilizing a DJI Mavic 3 PRO drone, because airplanes and other flying targets are logistically too difficult to arrange for this thesis. Drone used is shown in Figure 21.

Figure 21: *Drone used for testing (DJI Mavic 3 PRO)*

Relevant specifications for this drone were measured and the drone weights 958 g and has dimensions of: $347.5 * 290.8 * 107.7\ \mathrm{mm}$. Drone will be flown with pre-programmed route with all of these different modes and speed will be kept constant to make systematic tests without changing aspects between different resolutions. Drone's heading was kept constant during these tests so that RCS change would be minimal during the test. Radar location and flight route are shown in Figure 22.

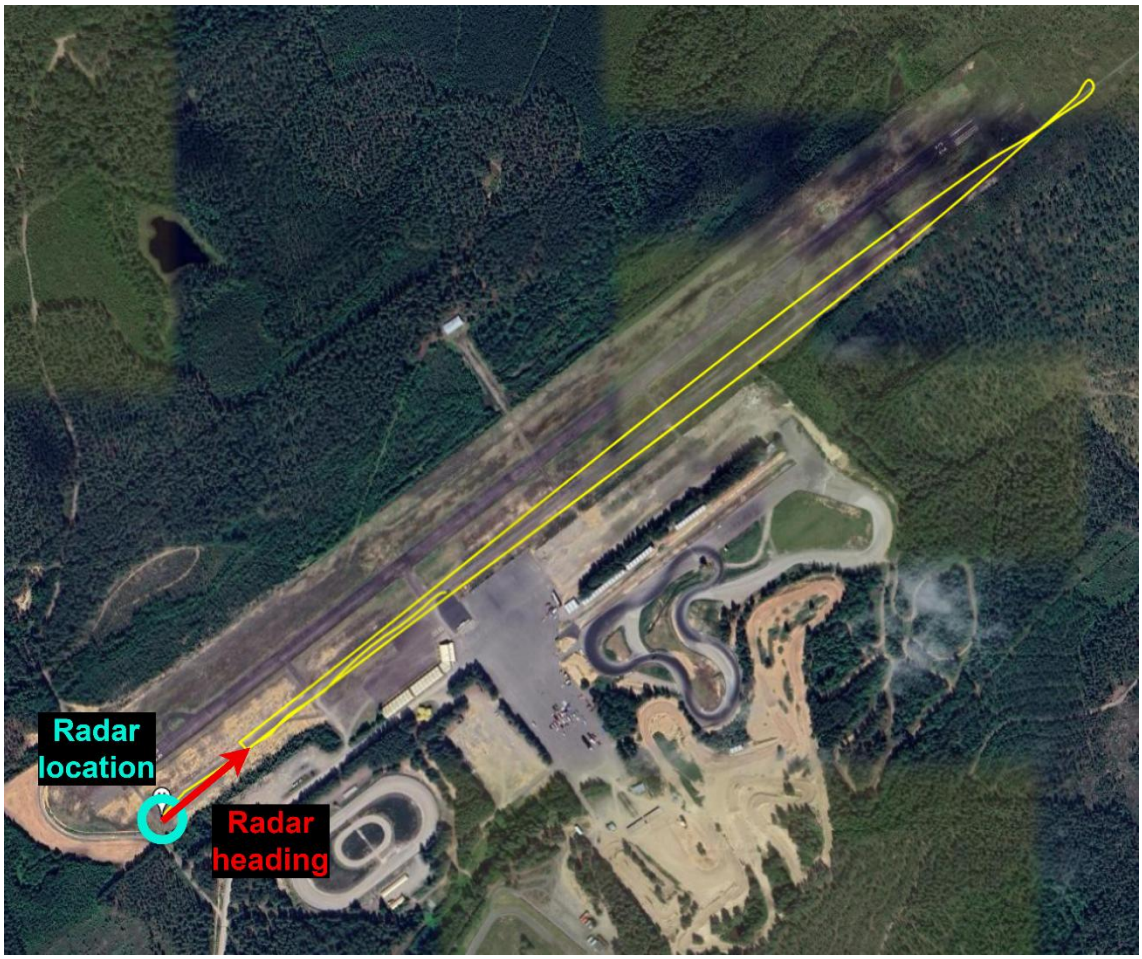

Figure 22: *Drone flight route and radar location*

Flight route shown here is collected from drone's locating system after the tests. This pre-controlled flight route was flown at constant speed for each of the tests. Area utilized for testing is Teisko Airport.

From these test results we can also get RCS estimate for the target drone. It will be constant during these different resolutions tested, and changes in results should be happening because integration gain changes.

This test was performed with different range and Doppler resolutions. Range resolutions will be ranging from 0.75 m to 5 m and Doppler resolutions will be ranging from 0.13 m/s to 0.88 m/s. Different range resolution modes are represented in Table 4:

Parameter	Range Mode 1	Range Mode 2	Range Mode 3	Range Mode 4	Range Mode 5	Range Mode 6
ΔR (m)	5	3	2.14	1.5	1.25	0.75
Δv_{r} (m/s)	0.11	0.11	0.11	0.11	0.11	0.11
t_{i} (ms)	102.4	102.4	102.4	102.4	102.4	102.4

Table 4: *Different range resolution modes*

Parameter	Doppler Mode 1	Doppler Mode 2	Doppler Mode 3	Doppler Mode 4	Doppler Mode 5	Doppler Mode 6
ΔR (m)	3	3	3	3	3	3
Δv_{r} (m/s)	0.88	0.44	0.25	0.18	0.15	0.13
t_{i} (ms)	10	20	36	48	60	68

Table 5: *Different Doppler resolution modes*

During range resolution tests the Doppler resolution was set constant, to see how range resolution affects detection SNR. Different Doppler resolution modes were also tested, which are represented in Table 5. In these later tests we can see that Doppler resolution has been changed between tests and based on equation (50), we know that Doppler resolution will only change when changing the integration time t_{i}. This means the integration gain will change because of this, but we can still see how resolution affects it, because SNR should change linearly with integration time and if it does not, it means that resolution made a difference on the results.

Results from these tests will then be extrapolated to airplanes and estimation on maximum detection range for airplanes with these different resolutions will be provided based on this data. Airplane RCS estimation of $\mathrm{RCS} = 100\ \mathrm{m}^2$ will be used for this extrapolation. This example value is for jumbo jet sized airplanes. [23]

To do this we can change equation (51) to show our maximum detection range. This maximum detection distance equation becomes:

$$R_{\max} = \left(\frac{P_{\mathrm{T}} G_{\mathrm{T}} G_{\mathrm{R}} \lambda^2 * \mathrm{RCS} * t_{\mathrm{i}}}{(4\pi)^3 \mathrm{SNR}_{\mathrm{th}} L_{\mathrm{a}} k T F_{\mathrm{n}} L_{\mathrm{T}}} \right)^{\frac{1}{4}} \tag{53}$$

In this test the target was moving over pre-programmed route as shown in Figure 18. Radar was operated with different resolutions and these results will be used to estimate RCS value for the drone. Temperature sensor reading during these tests stayed constant at $T_{\mathrm{R}} = 18\ ^{\circ}\mathrm{C}$, which makes the thermal loss to be $L_{\mathrm{T}} = 0.04\ \mathrm{dB}$. This resolution test was made for 6 different Doppler resolutions and 6 different range resolutions. Some difference between approaching and receding target was seen during testing, so for each mode both directions are graphed separately. Raw data looks very messy, as seen from Figure 23.

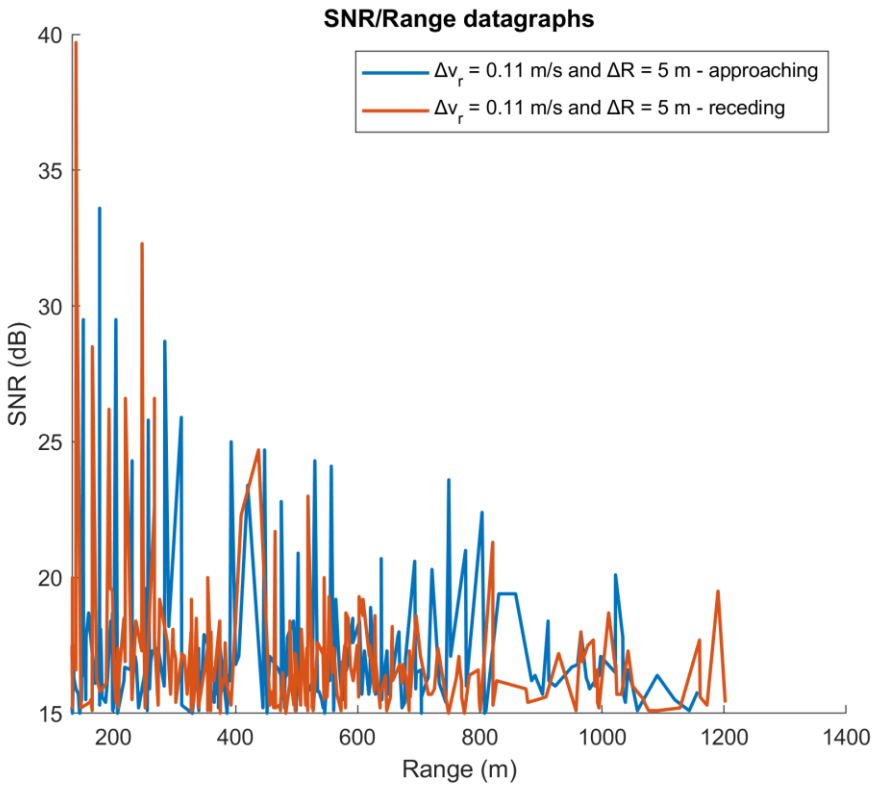

Figure 23: *Range/SNR data figure for Range resolution of 5 m*

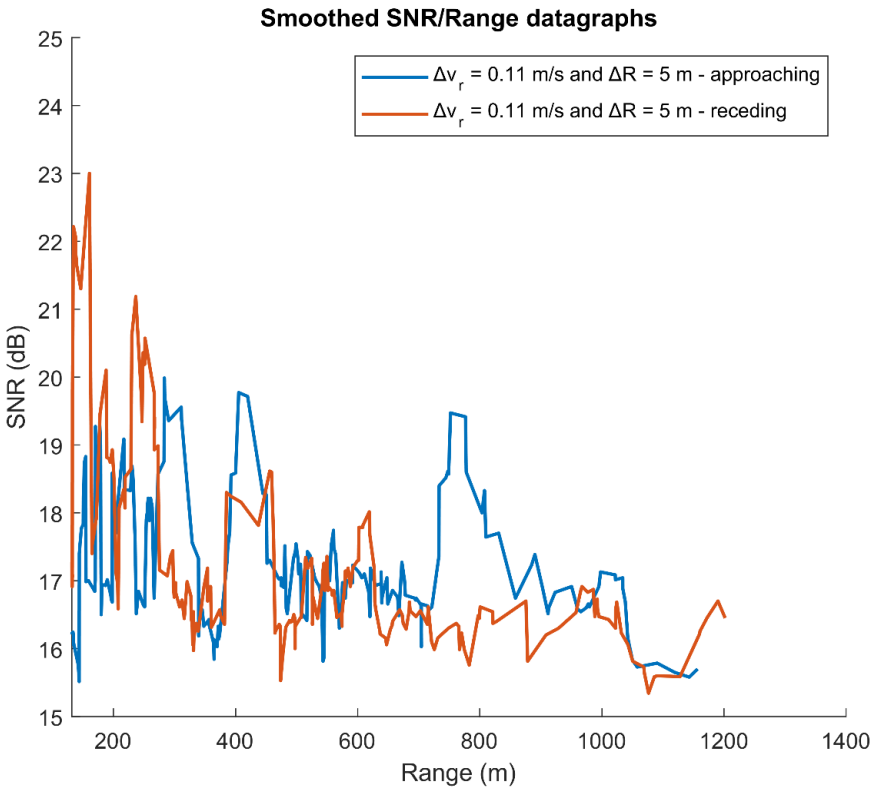

Figure 24: *Smoothed Range/SNR data figure for Range resolution of 5 m*

Because of how much variation there is in SNR/Range data, moving average of data was used to create cleaner graphs. Average of five adjacent datapoints was calculated and drawn on the graph. This cleans figure out a lot as seen in Figure 24. This way the figure looks a lot cleaner and this smoothening will be used to visualize data from all different resolutions measured. All approaching data is shown on Figure 25 and receding data on Figure 26.

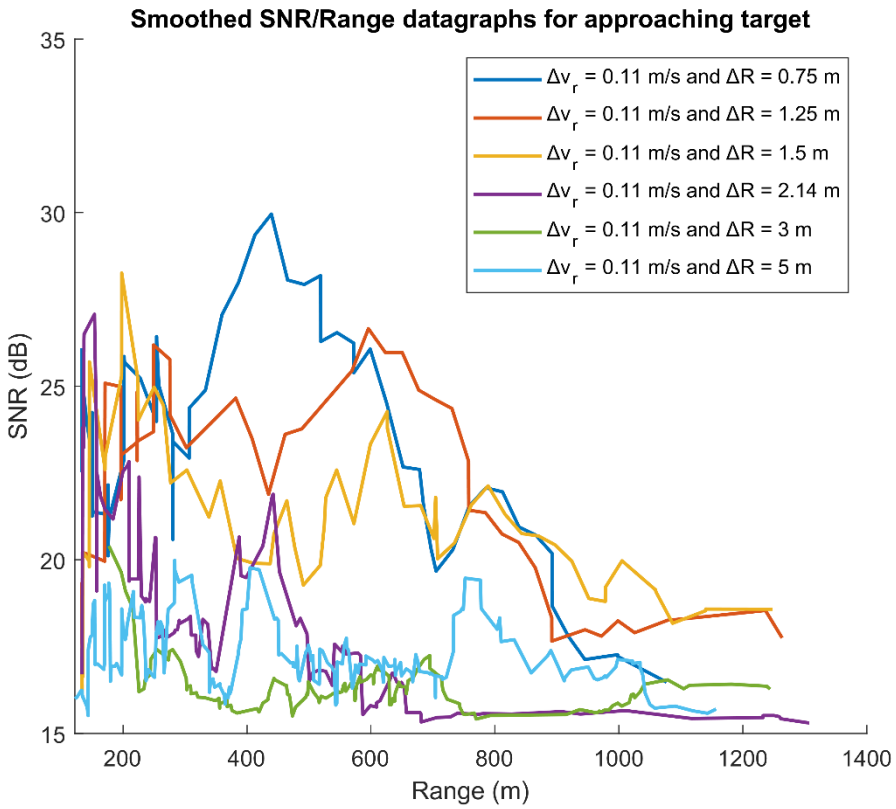

Figure 25: *Smoothed SNR/Range figures for range resolutions, approaching target*

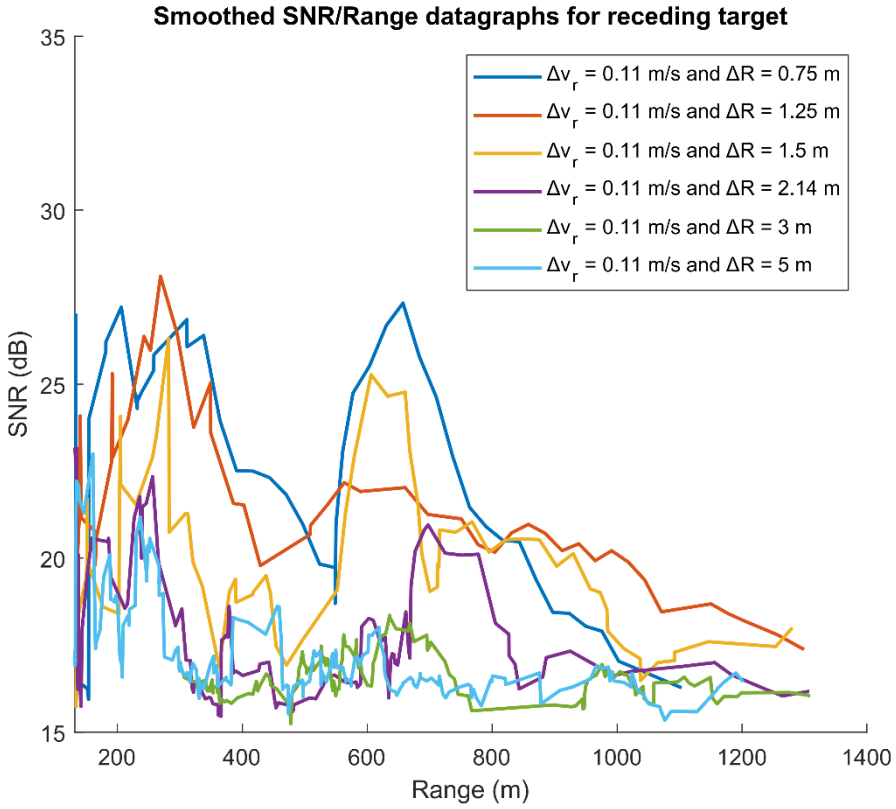

Figure 26: *Smoothed SNR/Range figures for range resolutions, receding target*

In Figures 25 and 26 we can see that there are clear differences between different range resolutions. Finest resolution of 0.75 m seems to fluctuate a lot, while resolution of 1.25 m seems to have highest SNR for detections with higher ranges and least fluctuation. These same plots were drawn for Doppler resolutions introduced in Table 5 and can be seen in Figures 27 and 28.

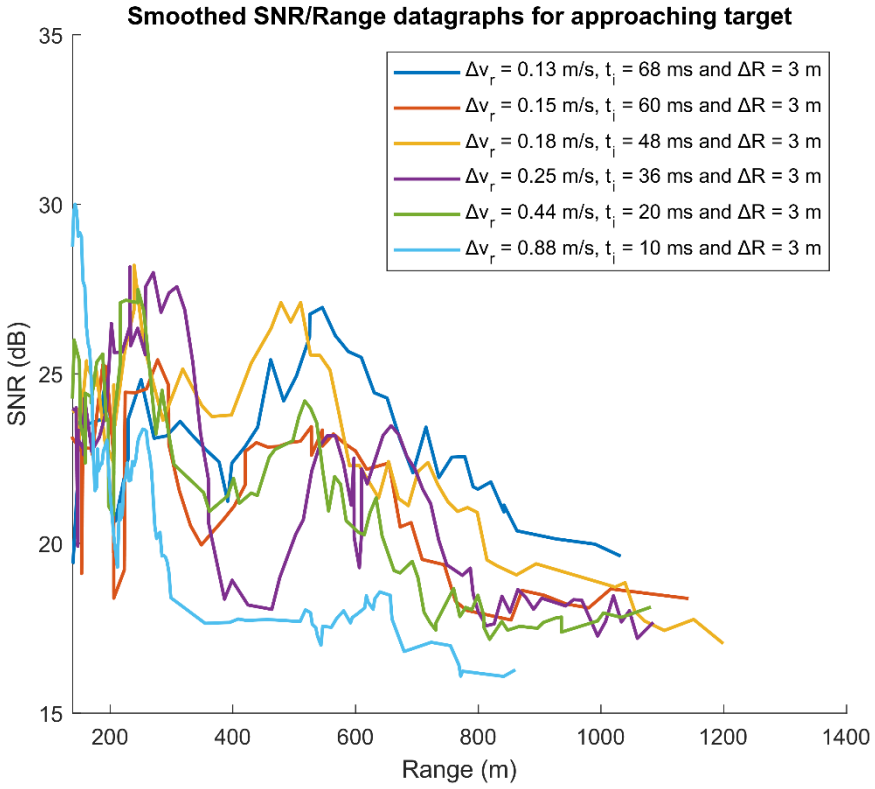

Figure 27: *Smoothed SNR/Range figures for Doppler resolutions, approaching target*

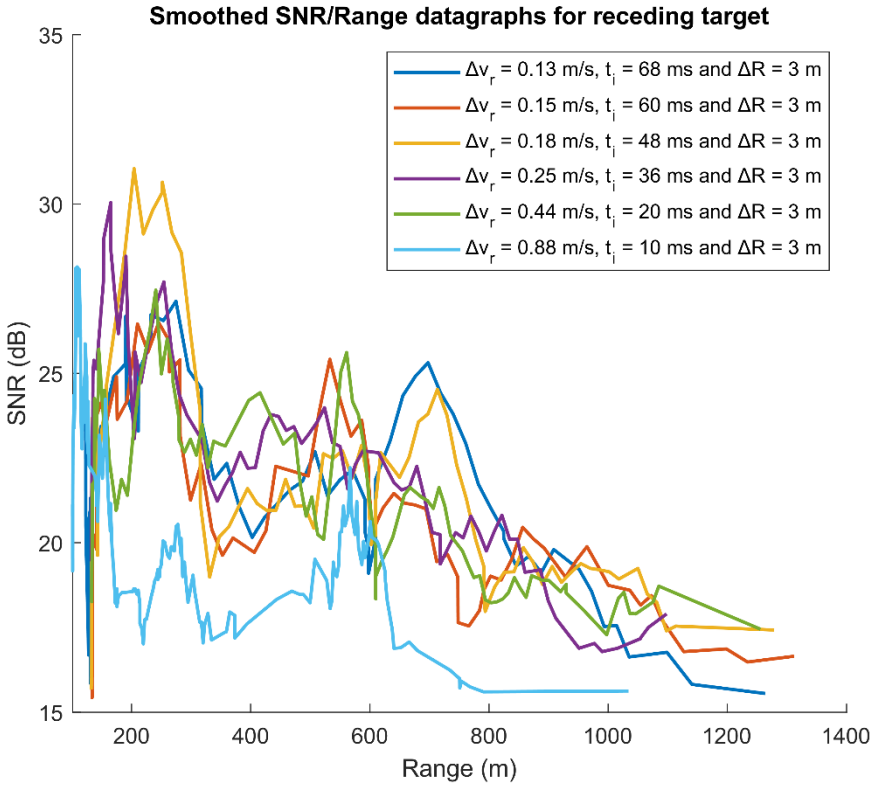

Figure 28: *Smoothed SNR/Range figures for Doppler resolutions, receding target*

In Figures 27 and 28 we can see that there was a lot of differences between Doppler resolutions. This can be because of many different reasons. One of the most likely reason is that drone's aspect was not staying constant between all resolutions. There most likely was little aspect changes happening to the drone, which can be because of changing wind conditions.

However, we can see that SNR values from these different Doppler resolutions do not change linearly with integration time as they should if integration is done as intended where the target stays in single cell over the whole integration time. This means that Doppler resolution does play a part in this SNR, where too fine Doppler and range resolution can lead to less SNR, even though longer integration time should increase SNR from the target.

Integration time t_i used in corner reflector testing was 25.6 ms and range resolution testing was done with integration time of 102.4 ms, while Doppler resolution testing has integration time changing from resolution to resolution. These differences in integration time will be noted in the calculations to get RCS estimation as accurate as possible. Temperatures read from the radar's temperature sensor were close to each other, 18 °C and 19 °C so no notable difference in thermal losses between these two test scenarios.

These RCS estimates will be calculated with data from the corner reflector calibration tests. We can calculate what SNR these measurements would lead to at different ranges and use that to estimate target RCS. SNR lowering over range can be calculated with:

$$\Delta\mathrm{SNR} = -40\log_{10}(R_{\mathrm{M}}) \tag{54}$$

where R_{M} is range multiplier, which tells how many times bigger new range is when compared to old known one. So from these three different corner reflector measurements we can conclude an estimation for detection RCS. All of these three different corner reflector measurements give bit different results. SNR/Range graphs for these corner reflectors is shown in Figure 29.

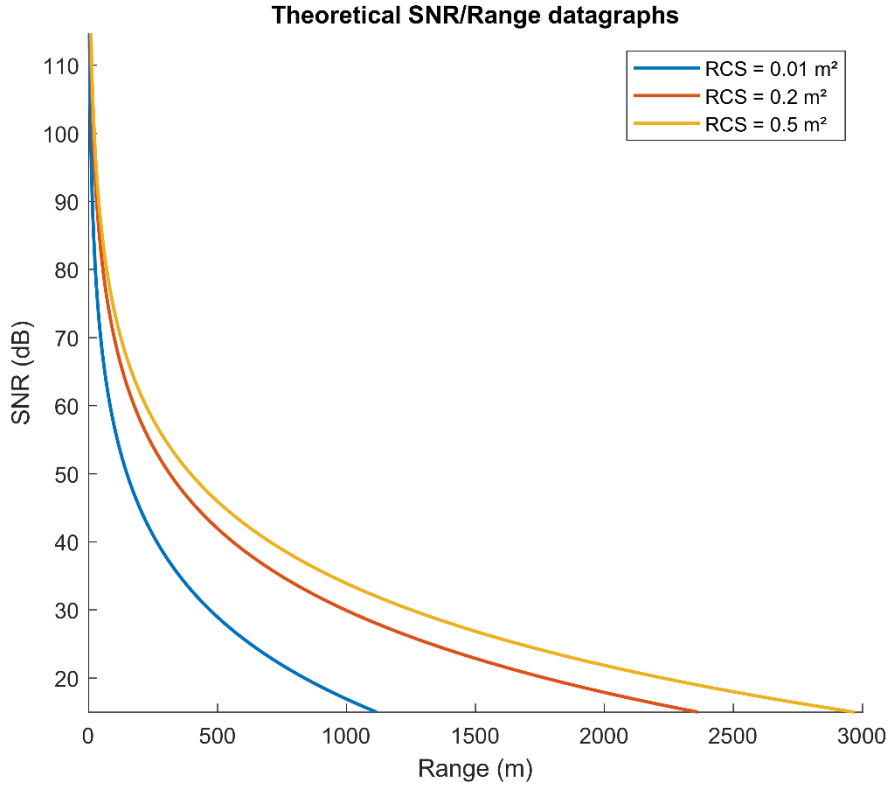

Figure 29: *Theoretical SNR/Range graphs for measured corner reflectors*

Now from here we can calculate estimate for each detection RCS with data known

$$\mathrm{RCS}_{\mathrm{est}} = \mathrm{RCS}_{\mathrm{cr}} 10^{\frac{\mathrm{SNR}_{\mathrm{det}} - \mathrm{SNR}_{\mathrm{cr}} + 4\log_{10}\left(\frac{R_{\mathrm{det}}}{R_{\mathrm{cr}}}\right)}{10}} \left(\frac{1}{\frac{t_{\mathrm{i,det}}}{t_{\mathrm{i,cr}}}} \right) \tag{55}$$

In equation (55) $\mathrm{RCS}_{\mathrm{cr}}$ is known RCS of corner reflector, $\mathrm{SNR}_{\mathrm{det}}$ is SNR from any target detection at distance R_{det}, $\mathrm{SNR}_{\mathrm{cr}}$ is SNR from corner reflector measurement done at distance R_{cr}. $t_{\mathrm{i,det}}$ is integration time used in resolution test and $t_{\mathrm{i,cr}}$ is integration time

used in corner reflector test. This equation can now be utilized to calculate RCS estimates from all resolution test detections.

With these results we are able to estimate target's RCS values from all of these detections by utilizing data gathered from corner reflector measurements earlier. With range, RCS and SNR values from Table 3 we can calculate RCS estimate from each resolution test data. This calculation will be done for raw data and smoothed with same technique used in Figures 25-28.

Corner reflector measurement results from all three measurements were used to calculate RCS estimate for the target. Average of these three values is used to draw graphs in Figures 30-33.

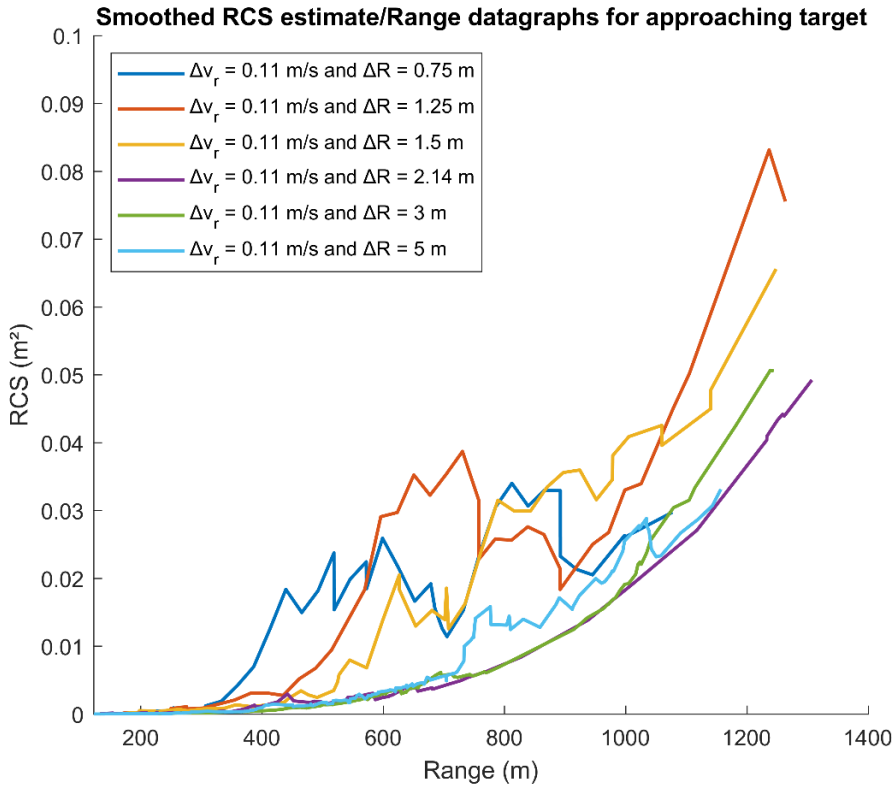

Figure 30: *RCS estimations for range resolutions, approaching target*

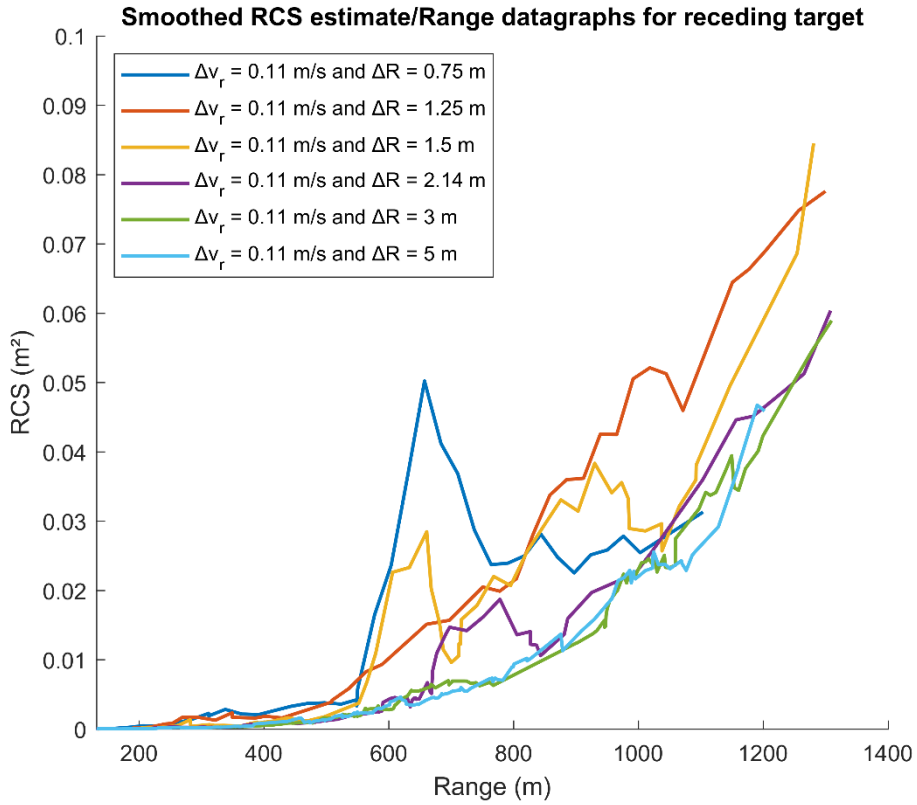

Figure 31: *RCS estimations for range resolutions, receding target*

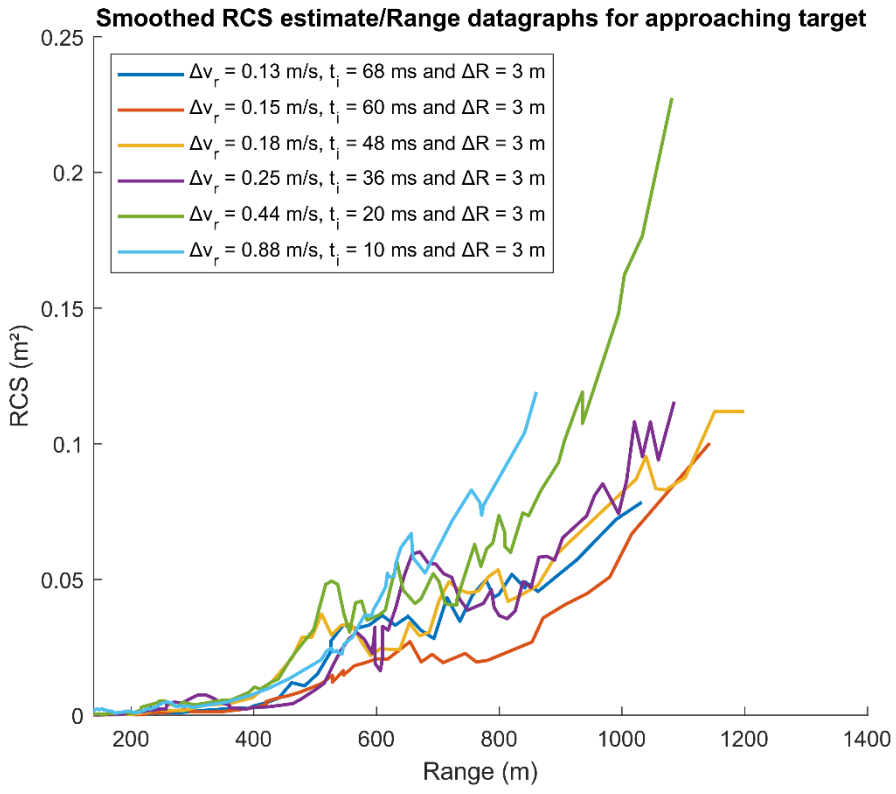

Figure 32: *RCS estimations for Doppler resolutions, approaching target*

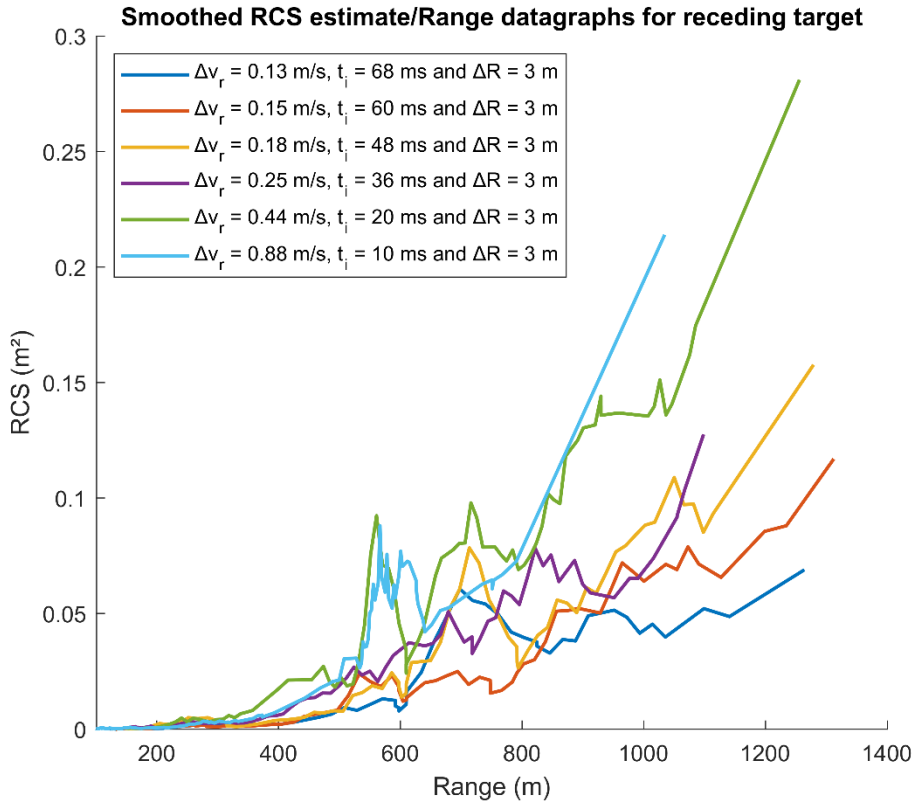

Figure 33: *RCS estimations for Doppler resolutions, receding target*

From Figures 30-33 we can see that RCS estimation is very low for shorter ranges and increases towards longer ranges. This can be partly explained with the fact that SNR fluctuates a lot and for shorter ranges the target is detected even when RCS is lower, but for longer ranges the target is only detected when RCS is high and that increases RCS estimate a lot when range increases. This is even more noticeable for different Doppler resolutions, because shorter integration time means integration gain is considered to be lower, but still target was detected from a long range. On top of that, these RCS estimations shows that integration time clearly does not give as much improvement in SNR as hoped, and shorter integration time can be even better, because it means targets can be detected more often without losing barely any SNR while doing so.

This however does not explain this big of an increase in RCS estimates, part of this has to be some unknown functionality of the radar. One explanation for this is that adaptive gain control (AGC) might be in use, which lowers front-end gain, when strong signal is received. This is done to ensure that ADC stays operating on dynamic range and not saturate, which leads to clipping. Adaptive gain control can also increase gain when weak signal is received to make it stay above the noise floor. This means that equation (10) has to include adaptive gain control as well, which changes it to:

$$\mathrm{SNR} = \frac{P_\mathrm{T} G_\mathrm{T} G_\mathrm{R} G_\mathrm{AGC} \lambda^2 \mathrm{RCS} G_\mathrm{i}}{(4\pi)^3 R^4 L_\mathrm{a} k T B F_\mathrm{n}} \tag{56}$$

Here G_AGC is gain from AGC, which will be estimated according data represented in Figures 30-33. This is done by using corner reflector measurement reference data and calculating estimated SNR for RCS estimates median value. AGC gain estimates are represented in Figures 34-37.

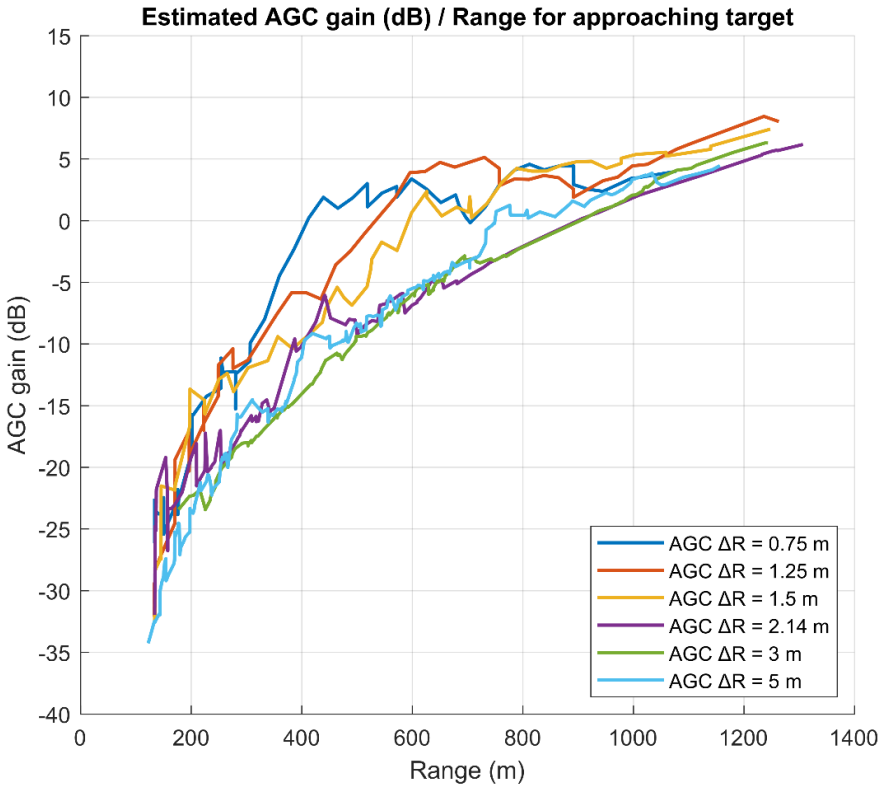

Figure 34: *AGC gain/Range estimate with range resolutions for approaching target*

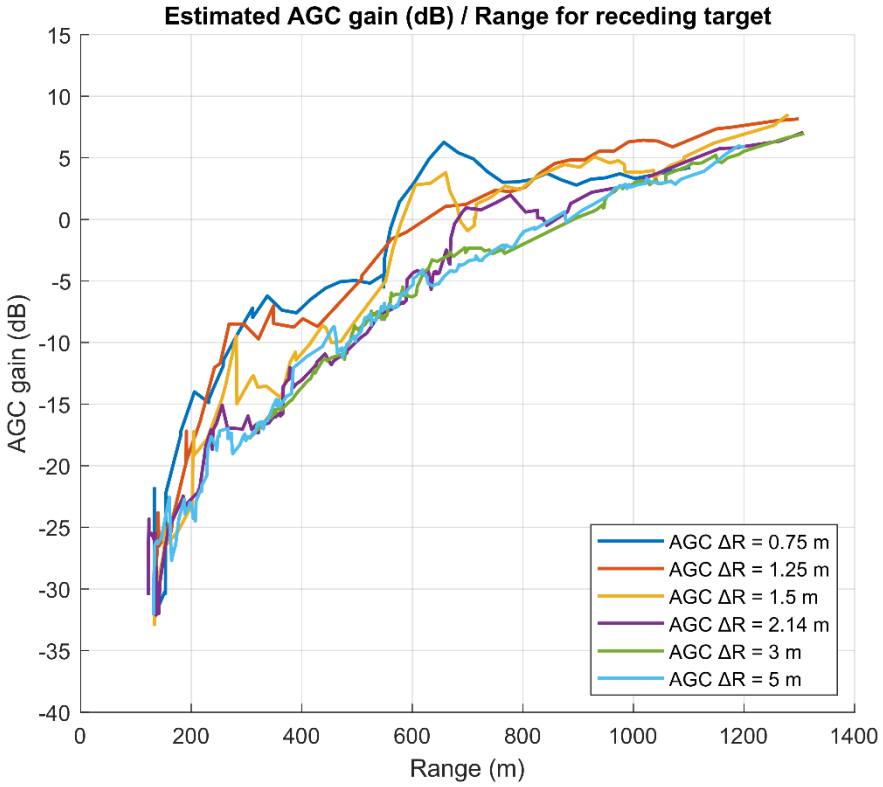

Figure 35: *AGC gain/Range estimate with range resolutions for receding target*

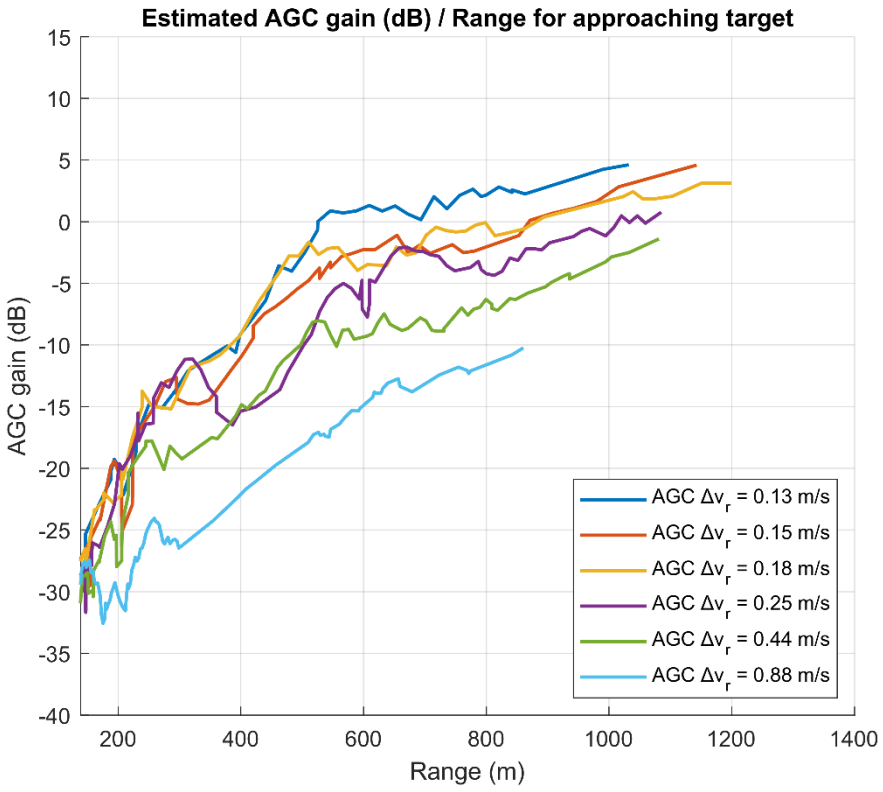

Figure 36: *AGC gain/Range estimate with Doppler resolutions for approaching target*

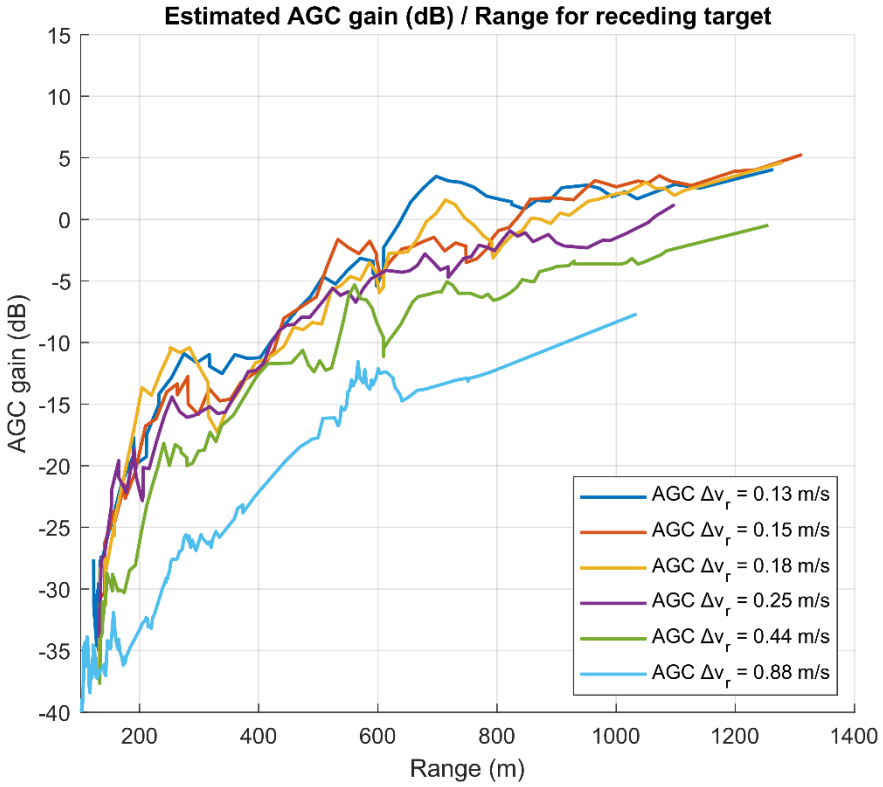

Figure 37: *AGC gain/Range estimate with Doppler resolutions for receding target*

Figures 34-37 provide data on estimated AGC gain over different ranges. With this we can see that there seems to be AGC, or similar system, which is causing detection SNR values to be inconsistent when compared to equation (10). Difference created by this additional gain modifier is around 40 dB from lowest to highest gain and this is why RCS estimations are increasing when the range increases. With this AGC correction, RCS estimates can now be scaled to correct levels. This correction was applied to every data-point. Histogram of different RCS estimates and frequency from all measurement data can be seen in Figure 38.

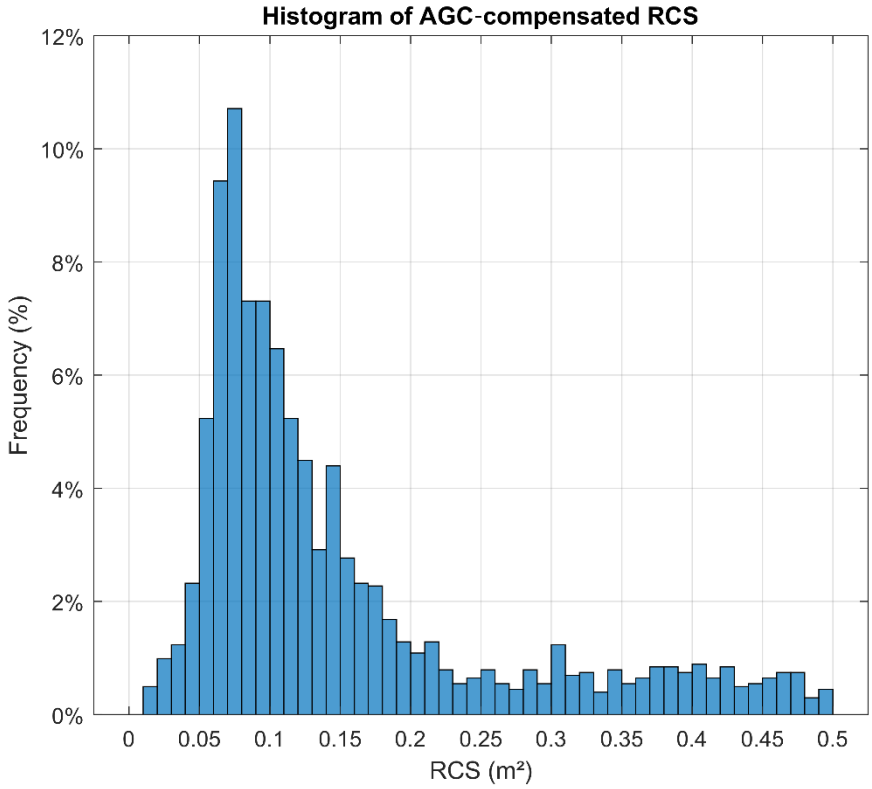

Figure 38: *AGC gain/Range estimate with Doppler resolutions for receding target*

According to Figure 38, RCS estimates are now concentrated between 0.05 and 0.1 m^2. RCS estimates can range all the way up to 0.5 m^2, this wide range of estimates most likely results from taking means of data between calculations, and also the fact that RCS does not stay constant, it changes so much depending on aspect, so some variance in the results is to be expected. The most common bin of the histogram is between 0.07 m^2 and 0.08 m^2, average of this data is 0.1504 m^2 and median comes out to 0.1067 m^2.

Now with these RCS estimations we can take a weighted mean and extrapolate the data to estimate how far target with RCS of $100\ \mathrm{m}^2$ would be visible. AGC calibration was not considered for this, because extrapolation depends on measured SNR. Weighted mean of RCS estimates was used from each dataset. This RCS estimate was then used for calculation.

$$\mathrm{SNR}_{100} = \mathrm{SNR}_{\mathrm{det}} - 10 * \log_{10}\left(\frac{\mathrm{RCS}_{\mathrm{est}}}{100}\right) \tag{57}$$

SNR for this larger target can be calculated with equation (57), where SNR_{100} is resulting SNR from large target, $\mathrm{SNR}_{\mathrm{det}}$ is SNR from detection during resolution test and $\mathrm{RCS}_{\mathrm{est}}$ is RCS estimate from same detection where $\mathrm{SNR}_{\mathrm{det}}$ is from. When this is combined with equation (53) we can calculate maximum range, where SNR for target with RCS of $100\ \mathrm{m}^2$ is 15 dB.

$$R_{100} = R_{\mathrm{det}} 10^{\left(\frac{\mathrm{SNR_{det}} - 15 - 10\left(\frac{\mathrm{RCS_{est}}}{100}\right)}{40}\right)} \quad (58)$$

In equation (58) $\mathrm{SNR_{det}}$ is SNR value from target detection measured during resolution testing and R_{det} is range from that detection. $\mathrm{RCS_{est}}$ is estimated RCS from the detection. This then results in maximum range where SNR is 15 dB.

Graphing maximum detection range from all detections would result in massive number of different graphs, so for these graphs all RCS estimates, SNR values and range values will be averaged from a dataset and with that average a maximum detection range for larger target is calculated. This data is either based on data gathered from approaching or receding target and will be shown separately, depending on which data it is based on. Then SNR/Range graph will be plotted according to equation (53). These graphs are shown in Figures 39-42.

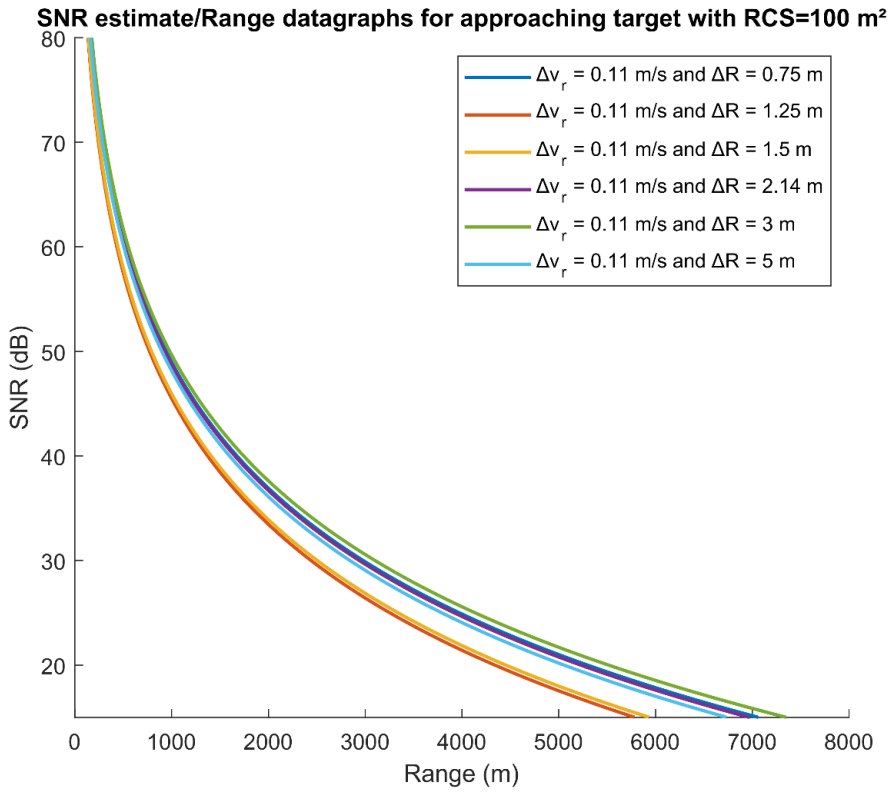

Figure 39: *SNR/Range estimate with range resolutions for large approaching target*

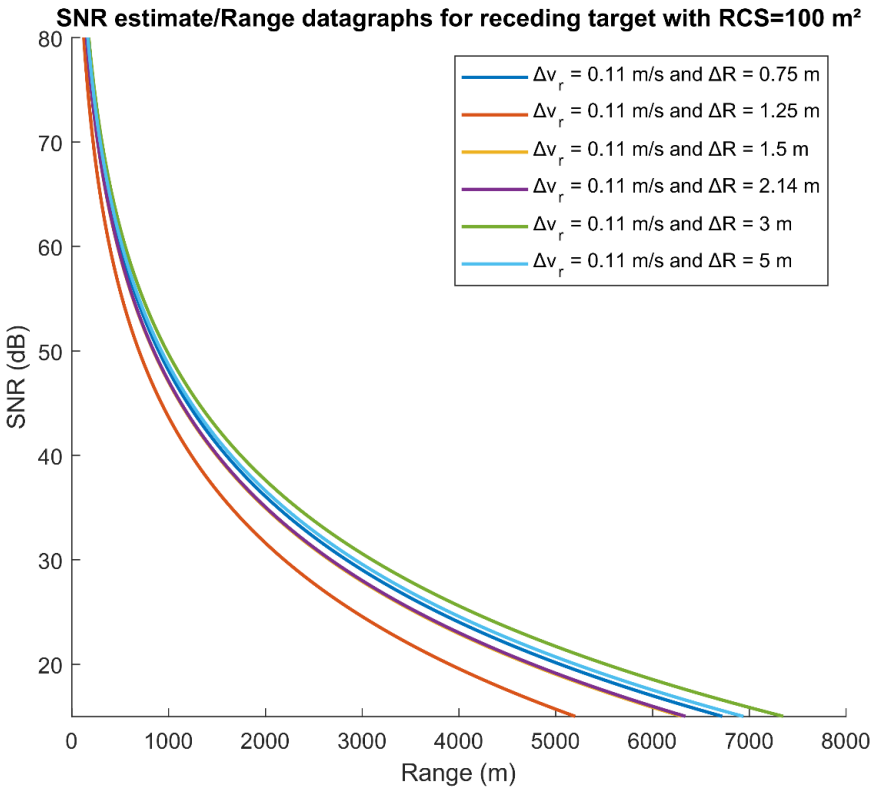

Figure 40: *SNR/Range estimate with range resolutions for large receding target*

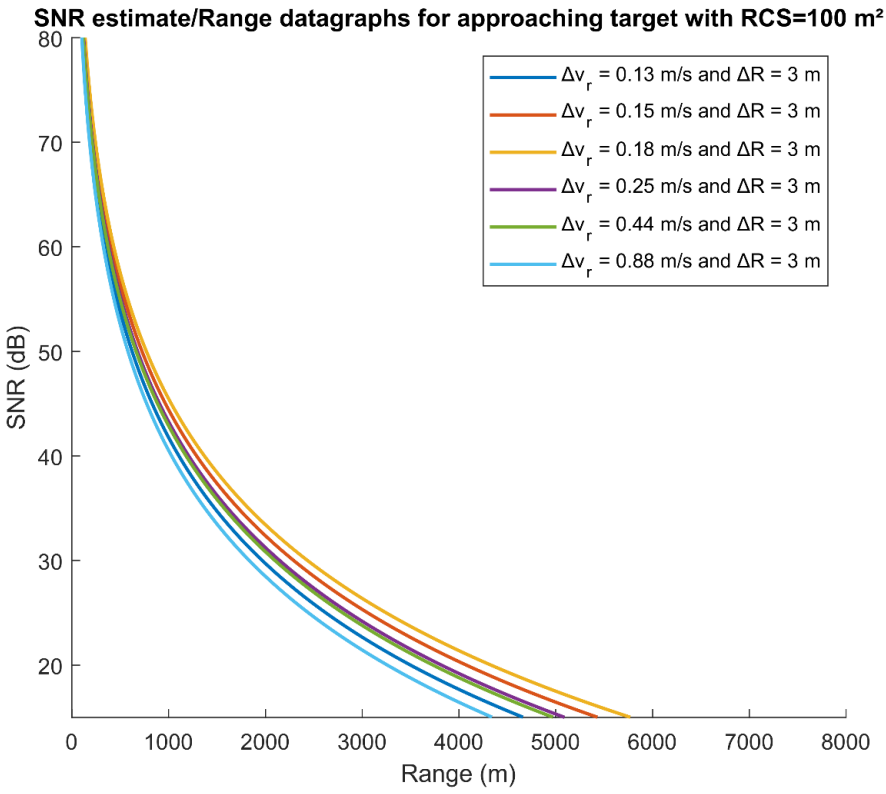

Figure 41: *SNR/Range estimate with Doppler resolutions for large approaching target*

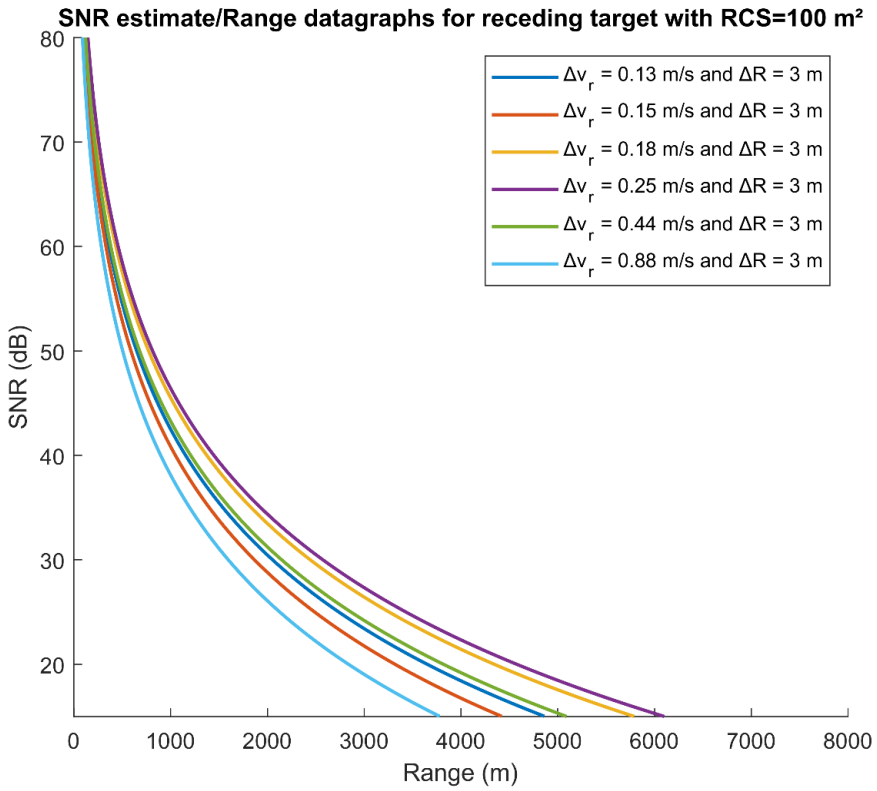

Figure 42: *SNR/Range estimate with Doppler resolutions for large receding target*

From Figures 39-42 we can see that estimates for larger target detection are ranging from 3700 m to 7300 m depending on the mode used. These estimates give a rough estimation range for a maximum detection distance with the radar. Average of these estimations is 5500 m, but depending on resolutions used and weather conditions, larger objects can be detected as far as 7300 m. Clear differences between resolutions can be seen especially in maximum range estimations. One crucial factor for this is the fact that integration time did not increase SNR as much as hoped. This leads to a significantly higher RCS estimations for Doppler resolutions with shorter integration time. These problems with resolutions can act differently when utilizing larger target compared to a small drone.

CONCLUSIONS

Field testing can be a very useful tool for radar characterization, because it provides actual real life performance data, which includes non-idealities that result from environment. Field testing requires a lot of planning and there are factors that affect the results, but cannot be controlled, like the weather, which affects thermal noise and transmit power loss within the radar itself. This has to be kept in mind when analysing the results and need to be compensated to obtain correct information about radar performance. Weather conditions like rain or snow can add clutter to the radar FOV or attenuate the transmit signal. This means that controlled tests should be done during the same day and weather should be as similar as possible between different tests to provide accurate results.

Characterization can focus on any performance aspect of a radar and this characterization process can be made very comprehensive. This can include, but are not limited to: angle resolutions in azimuth and elevation direction, range resolution and Doppler resolution. These can of course be calculated, but field testing provides great data on how theoretical values compare against the radar's real performance. This thesis was done to provide data about how simple characterization results for a radar can be provided with field testing and I think that goal was well achieved.

Characterization tests done in this thesis are few, which were deemed the most important. These tests focused on different aspects of the radar's performance. First test focused on temperature's effect on transmit power, which shows that transmit power lowers by 3 dB when internal temperature of the radar reaches $65\,^{\circ}\mathrm{C}$. During this test radar's antenna pattern was also measured. After that the radar's received signal data was calibrated with corner reflectors. After those different resolutions were tested to see how resolutions affect received SNR from target. According to the results from data calibration and resolution testing, the radar should be able to detect a large aircraft at a range of approximately 5500 m.

For better results characterization tests should first be done in more controlled environment and after that move to field testing to see how the performance differs from ideal situation, but for this thesis field testing was used to see how well field testing fits radar characterization needs. For this scenario field testing proved to be a good way to approach this radar characterization problem. These results could have been made more comprehensive by utilizing more targets with different RCS values, which would have

improved results and accuracy of the estimates provided for the radar. If characterization was to continue from here, one thing that would most definitely be on the list is seeing how much integration gain differs from theoretical value. Adaptive gain control would need to be tested more in-depth too. These could then be used to get more accurate results from this resolution testing. Then a larger target could be utilized to accurately test if this theoretical maximum would apply to a real-world scenario and to see how different resolutions would act with a larger target.

REFERENCES

[1] Wolf, C. “Radartutorial, Book 1 “Radar Basics””, 2009. URL: https://www.radartutorial.eu/druck/Book1.pdf (Accessed 3.9.2025)

[2] Bhatta, N. P. and Geethapriya, M. RADAR and its Applications, 2017. URL: https://www.researchgate.net/publication/317427496_RADAR_and_its_Applications (Accessed 3.9.2025)

[3] NOVELIC. ”Radar characterization”. URL: https://www.novelic.com/radar-characterization/ (Accessed 20.10.2025)

[4] Richards, M. A. Fundamentals of Radar Signal Processing. 2nd ed., 2014.

[5] Tse, D. and Viswanath, P. Fundamentals of Wireless Communication, 2005. pp 10-42

[6] Wolf, C. Free-Space Path Loss (FSPL), radartutorial.eu, URL: https://www.radartutorial.eu/01.basics/Free-Space%20Path%20Loss.en.html (Accessed 23.9.2025)

[7] Kannanthara, J., Griffiths, D., Jahangir, M., Jones, J. M., Baker, C. J., Antoniou, M., Bell, C. J., White, H., Bongs, K., Singh, Y. Whole system radar modelling: Simulation and validation, 2023. URL: https://doi.org/10.1049/rsn2.12399 (Accessed 3.9.2025)

[8] NIST. “SI Redefinition”, 2018. URL: https://www.nist.gov/si-redefinition (Accessed 3.9.2025)

[9] Wolf, C. “Noise”, URL: https://www.radartutorial.eu/18.explanations/ex08.en.html (Accessed 17.9.2025)

[10] ITU. Recommendation ITU-R P.372-13 Radio noise, 2016. URL: https://www.itu.int/dms_pubrec/itu-r/rec/p/R-REC-P.372-13-201609-S!!PDF-E.pdf (Accessed 17.9.2025)

[11] Richards, M. A., Scheer, J. A., Holm, W. A. Principles of Modern Radar: Basic principles, 2010. URL: https://doi.org/10.1049/SBRA021E, pp 70, 165-207,347-390, 536-538, 625-673, 697-699, 787-794

[12] Kronauge, M. Waveform Design for Continuous Wave Radars. 1st ed., 2014. pp 15-19

[13] Alabaster, C. Pulse Doppler Radar: Principles, Technology, Applications., 2012. pp 25-42, 82

[14] Forsten, H. “Homemade 6 GHz pulse compression radar”. 2024. URL: https://hforsten.com/homemade-6-ghz-pulse-compression-radar.html (Accessed on 23.10.2025)

[15] Wolf, C.”Continuous Wave Radar”, URL: https://www.radartutorial.eu/02.basics/Continuous%20Wave%20Radar.en.html (Accessed 4.8.2025)

[16] Melvin, W. L. and Scheer, J. A. Principles of Modern Radar. Volume III, Radar Applications. 2014. pp 17-81

[17] Melvin, W. L. and Scheer, J. A. Principles of Modern Radar: Advanced Techniques. 2013. URL: https://doi.org/10.1049/SBRA020E, pp 119-142

[18] Rao, S. MIMO Radar, 2018. URL: https://www.ti.com/lit/pdf/swra554

[19] Doan, V., Huynh-The, T., Hoang, V., Vesely, J. “Phase-difference Measurement-based Angle of Arrival Estimation Using Long-baseline Interferometer.” *IET Radar, Sonar & Navigation*, vol. 17, no. 3. 2023. URL: https://doi.org/10.1049/rsn2.12352, pp. 449–465

[20] Jiao, Y., Zhang, F., Huang, Q., Liu, X., Li, L. Analysis of Interpolation Methods in the Validation of Backscattering Coefficient Products. 2023. URL: https://doi.org/10.3390/s23010469

[21] Jeffrey, T. Phased-Array Radar Design: Application of Radar Fundamentals, 2009. pp 17-25

[22] Budge, M. C. and German, S. R. Basic radar tracking. 1st ed. 2018, pp 1-2

[23] MIT Lincoln Laboratory, “Introduction to Radar Systems Target Radar Cross Section”. URL: https://www.ll.mit.edu/sites/default/files/outreach/doc/2018-07/lecture%204.pdf